Supporting Information

Synthesis, Photophysics and Switchable Luminescence Properties of a New Class of Ruthenium(II)-Terpyridine Complexes Containing Photoisomerizable Styrylbenzene Units

Poulami Pal,[†] Shruti Mukherjee,[†] Dinesh Maity[†‡] and Sujoy Baitalik[*†]

[†]Department of Chemistry, Inorganic Chemistry Section, Jadavpur University,

Kolkata 700032, India.

[‡] Department of Chemistry, Katwa College, Purba Bardhaman, West Bengal,

Pin-713130, India

Physical Measurements. Elemental analyses of the compounds were performed with a Vario-Micro V2.0.11 elemental (CHNSO) analyzer. NMR spectra were collected on a Bruker 300 MHz spectrometer in $CDCl_3$ for the ligands and in DMSO-d_6 for the metal complexes. High resolution mass spectroscopy was performed on a Waters Xevo G2 QTOf mass spectrometer. The UV-vis absorption spectra were recorded with a Shimadzu UV 1800 spectrometer. Steady state luminescence spectra were obtained either by a Horiba Fluoromax-4 spectrometer. Luminescence quantum yields were determined by using literature method taking quinine $[Ru(bpy)_3]^{2+}$as the standard. Luminescence lifetime measurements were carried out by using time–correlated single photon counting set up from Horiba Jobin-Yvon. The luminescence decay data were collected on a Hamamatsu MCP photomultiplier (R3809) and were analyzed by using IBH DAS6 software.

Electrochemical measurements were carried out in deaerated acetonitrile with a BAS epsilon electrochemistry system and a three-electrode set up consisting of a platinum or glassy carbon working electrode, a platinum counter electrode, and Ag/AgCl reference electrode. In all the experiments, tetraethylammonium perchlorate (TEAP) was used as background electrolyte. The potentials reported in this study were referenced against the Ag/AgCl electrode, which under the given experimental conditions gave a value of 0.36 V for the Fc/Fc^+ couple.

Experimental uncertainties are as follows: absorption maxima, ±2 nm; molar absorption coefficients, 10%; emission maxima, ±5 nm; excited–state lifetimes, 10%; luminescence quantum yields, 20%.

Determination of *Trans*-*Cis* Photoisomerization Quantum Yields. A 1-cm light path length quartz cell was used for the photoisomerization measurements. The concentration of the complexes was maintained in the range of 0.6×10^{-5} M - 1.2×10^{-5} M, and the solution was thoroughly degassed with N_2 before photoirradiation and stirred magnetically during *trans*-to-*cis* isomerization. Isomerization studies were carried out in a photocatalytic reactor designed by Lelesil Innovative Systems by using both ultraviolet and visible light source. The rate constant of the isomerization process were evaluated from the absorbance titration data using equation (S1).[S1]

$$\ln\{(A_0 - A_f)/(A_t - A_f)\} = k_{iso}t \qquad \text{(S1)}$$

where A_0, A_t, and A_f is the absorbance of the free receptor, after time t, and at the conclusion of the reaction. K_{iso} is the rate constant of isomerization and t is the required time for the

completion of the isomerization process. Both k_{iso} and A_f were estimated by nonlinear least-square method. The intensity of the light source was ~0.11 W. Quantum yields (φ) of the isomerization process were obtained by using the equation,[S2]

$\nu = (\varphi I_0/V)(1\text{-}10^{-Abs)}$

where ν is the rate of the trans-to-cis isomerization, I_0 is the photon flux at the front of the cell, V is the volume of the solution, and Abs is the initial absorbance at the irradiation wavelength.

Computational Methods. All calculations were performed with the Gaussian 09 program[S3] employing the DFT method with Becke's three-parameter hybrid functional and Lee-Yang-Parr's gradient corrected correlation functional B3LYP level of theory.[S4-S5] 6-31G* and 6-311G* basis sets were employed for the C, H, N, and O while SDD basis set was used for Ru atom.[S6] Geometries were fully optimized using the criteria of the respective programs. TD-DFT[S7-S10] calculations of the singlet-singlet excitations were performed in acetonitrile simulated by the CPCM model[S11] by using the so-called nonequilibrium approach, which has been designed for the study of the absorption process.[S12-S13] We also perform the UKS calculations directly on the triplet state of the complexes to calculate singlet-triplet energy gap. Orbital analysis was completed with Gauss View[S14] and Gauss sum 2.2.[S15]

X-ray Crystal Structure Determination. Single crystals of **2** were grown by slow diffusion of toluene to its MeCN-DCM (1:5, v/v) solution. X–ray diffraction data for the crystal of **2** mounted on a glass fiber and coated with perfluoropolyether oil was collected on a Bruker–AXS SMART APEX II diffractometer at 293 K equipped with CCD detector using graphite–monochromated MoKα radiation (λ = 0.71073 Å). Crystallographic data and details of structure determination are summarized in Table S1. The data were processed with SAINT and absorption corrections were made with SADABS.[S16] The structure was solved by direct and Fourier methods and refined by full–matrix least–square based on F^2 using the WINGX software which utilizes SHELX–97.[S17] For the structure solution and refinement the SHELXTL software packages was used.[S18] The non hydrogen atoms were refined anisotropically, while the hydrogen atoms were placed with fixed thermal parameters at idealized positions. The electron density map indicate the presence of some unassignable peaks, which were removed by running the program SQUEEZE.[19] CCDC reference number: 1845653 for **2**.

Tables for Supporting Information

Table S1. Crystallographic Data for $[Ru(tpy\text{-}pvp\text{-}Me)_2](ClO_4)_2 \cdot PhCH_3$

Compound	**2**
Formula	$C_{67}H_{54}Cl_2N_6O_8Ru$
fw	1243.13
T (K)	293 K
Cryst. Syst.	Monoclinic
Space group	P2(1)/c
a (Å)	19.593(5)
b (Å)	17.367(5)
c (Å)	18.153(5)
α (deg)	90.000(5)
β (deg)	108.269(5)
γ (deg)	90.000(5)
V (Å^3)	5866(3)
Dc(g cm^{-3})	1.408
Z	4
μ (mm^{-1})	0.421
F(000)	2560.0
θ range (deg)	2.19-25.58
Data/restraints/params	13216/0/760
GOF on F^2	0.943
R_1 [$I > 2\sigma(I)$][a],	0.0419
wR_2 (all data)[b]	0.1339
$\Delta\rho_{max}/\Delta\rho_{min}$ (e Å)	1.169/ -0.599
[a]R1(F) = [$\sum \| F_0 \| - \|F_C\| / \sum \| F_0 \|$], [b]wR2 (F^2) = $[\sum w(F_0^2 - F_C^2)^2 / \sum w(F_0^2)^2]^{1/2}$	

Table S2. Selected Experimental and Calculated Bond Distances (Å) and Angles (deg) for **2**

	2		
	Exptl.	Soln (singlet)	Soln (triplet)
Ru1-N1	2.080(2)	2.112	2.116
Ru1-N6	2.071(2)	2.112	2.122
Ru1-N4	2.071(2)	2.112	2.122
Ru1-N3	2.059(2)	2.112	2.116
Ru1-N5	1.971(2)	2.007	1.958
Ru1-N2	1.973(2)	2.007	2.052
N1-Ru1-N6	97.0(8)	92.3	100.9
N1-Ru1-N4	89.4(8)	92.3	92.3
N6-Ru1-N4	157.8(8)	156.7	158.1
N1-Ru1-N3	157.7(8)	156.7	154.0
N6-Ru1-N3	87.0(8)	92.3	92.4
N4-Ru1-N3	94.8(8)	92.3	92.4
N1-Ru1-N5	103.7(8)	101.4	103.0
N6-Ru1-N5	78.9(8)	78.3	79.0
N4-Ru1-N5	78.9(8)	78.3	79.1
N3-Ru1-N5	98.5(8)	101.7	102.9
N1-Ru1-N2	78.5(8)	78.3	77.0
N6-Ru1-N2	101.7(8)	101.7	100.9
N4-Ru1-N2	100.3(8)	101.4	101.0
N3-Ru1-N2	79.2(8)	78.3	77.0
N5-Ru1-N2	177.6(8)	179.8	179.9

Table S3. Selected Calculated Bond Distances (Å) and Angles (deg) for $[(Ru(tpy\text{-}pvp\text{-}H)_2]^{2+}$ (**1**)

	1					
	Ground State			Excited State		
	Trans-trans	*Trans-cis*	*Cis-cis*	*Trans-trans*	*Trans-cis*	*Cis-cis*
Ru1-N1	2.112	2.112	2.111	2.119	2.112	2.112
Ru1-N6	2.112	2.111	2.111	2.113	2.120	2.120
Ru1-N4	2.112	2.111	2.111	2.111	2.119	2.119
Ru1-N3	2.112	2.111	2.110	2.118	2.112	2.112
Ru1-N5	2.008	2.007	2.006	2.050	2.054	2.054
Ru1-N2	2.008	2.008	2.007	1.955	1.955	1.955
N1-Ru1-N6	92.3	92.4	92.3	92.4	92.3	92.3
N1-Ru1-N4	92.2	92.2	92.2	92.4	92.4	92.4
N6-Ru1-N4	156.7	156.8	156.8	154.2	158.4	158.4
N1-Ru1-N3	156.7	156.7	156.8	158.3	153.9	153.9
N6-Ru1-N3	92.3	92.4	92.3	92.2	92.5	92.5
N4-Ru1-N3	92.3	92.3	92.3	92.4	92.2	92.2
N1-Ru1-N5	101.7	101.6	101.6	100.6	103.0	103.0
N6-Ru1-N5	78.4	78.4	78.4	77.1	79.2	79.2
N4-Ru1-N5	78.3	78.3	78.4	77.1	79.2	79.2
N3-Ru1-N5	101.4	101.6	101.5	100.9	102.9	102.9
N1-Ru1-N2	78.3	78.4	78.3	79.1	77.0	77.0
N6-Ru1-N2	101.4	101.2	101.8	103.1	100.5	100.5
N4-Ru1-N2	101.7	102.0	101.3	102.6	100.9	100.9
N3-Ru1-N2	78.4	78.4	78.4	79.1	76.9	76.9
N5-Ru1-N2	179.8	179.6	179.7	179.6	179.8	179.8

Table S4. Selected Calculated Bond Distances (Å) and Angles (deg) for $[(Ru(tpy\text{-}pvp\text{-}Cl)_2]^{2+}$ (**3**)

	3					
	Ground State			Excited State		
	Trans-trans	*Trans-cis*	*Cis-cis*	*Trans-trans*	*Trans-cis*	*Cis-cis*
Ru1-N1	2.112	2.112	2.111	2.119	2.120	2.112
Ru1-N6	2.112	2.112	2.112	2.112	2.112	2.118
Ru1-N4	2.112	2.112	2.110	2.111	2.112	2.120
Ru1-N3	2.112	2.111	2.111	2.118	2.119	2.112
Ru1-N5	2.007	2.008	2.007	2.051	2.051	2.054
Ru1-N2	2.007	2.008	2.007	1.955	1.955	1.955
N1-Ru1-N6	92.3	92.4	92.3	92.4	92.4	92.3
N1-Ru1-N4	92.2	92.3	92.3	92.4	92.6	92.5
N6-Ru1-N4	156.7	156.8	156.8	154.1	154.2	158.5
N1-Ru1-N3	156.7	156.7	156.7	158.4	158.4	153.9
N6-Ru1-N3	92.2	92.3	92.2	92.2	92.3	92.4
N4-Ru1-N3	92.2	92.3	92.3	92.4	92.3	92.5
N1-Ru1-N5	101.4	101.8	101.5	100.6	100.8	103.1
N6-Ru1-N5	78.3	78.4	78.3	77.0	77.1	79.2
N4-Ru1-N5	78.4	78.3	78.4	77.0	77.1	79.2
N3-Ru1-N5	101.7	101.4	101.6	100.6	100.8	102.9
N1-Ru1-N2	78.4	78.4	78.3	79.2	79.2	76.9
N6-Ru1-N2	101.7	101.2	101.8	102.6	102.8	100.8
N4-Ru1-N2	101.4	101.9	101.3	103.1	103.0	100.6
N3-Ru1-N2	78.3	78.4	78.3	79.2	79.2	76.9
N5-Ru1-N2	179.8	179.6	179.7	179.7	179.8	179.8

Table S5. Selected Calculated Bond Distances (Å) and Angles (deg) for $[(Ru(tpy\text{-}pvp\text{-}NO_2)_2]^{2+}$ (**4**)

	4					
	Ground State			Excited State		
	Trans-trans	*Trans-cis*	*Cis-cis*	*Trans-trans*	*Trans-cis*	*Cis-cis*
Ru1-N1	2.112	2.112	2.111	2.120	2.118	2.112
Ru1-N6	2.112	2.112	2.111	2.112	2.114	2.119
Ru1-N4	2.112	2.111	2.111	2.112	2.114	2.121
Ru1-N3	2.112	2.111	2.111	2.120	2.118	2.112
Ru1-N5	2.006	2.008	2.008	2.052	2.053	2.055
Ru1-N2	2.006	2.008	2.007	1.955	1.955	1.955
N1-Ru1-N6	92.3	92.3	92.3	92.3	92.4	92.2
N1-Ru1-N4	92.2	92.5	92.3	92.4	92.6	92.4
N6-Ru1-N4	156.8	156.8	156.8	154.0	154.2	158.3
N1-Ru1-N3	156.8	156.8	156.7	158.4	153.8	153.8
N6-Ru1-N3	92.3	92.3	92.2	92.3	92.3	92.4
N4-Ru1-N3	92.3	92.3	92.3	92.4	92.3	92.5
N1-Ru1-N5	101.7	101.7	101.5	100.6	100.8	103.1
N6-Ru1-N5	78.4	78.3	78.3	77.0	77.1	79.2
N4-Ru1-N5	78.3	78.4	78.4	77.0	77.1	79.2
N3-Ru1-N5	101.4	101.5	101.6	100.9	100.8	102.9
N1-Ru1-N2	78.3	78.4	78.4	79.2	79.2	76.9
N6-Ru1-N2	101.4	101.4	101.7	103.2	102.8	100.8
N4-Ru1-N2	101.7	101.8	101.4	102.6	103.1	100.6
N3-Ru1-N2	78.4	78.4	78.3	79.2	79.2	76.9
N5-Ru1-N2	179.8	179.7	179.8	179.6	179.8	179.8

Table S6. Selected Calculated Bond Distances (Å) and Angles (deg) for $[(Ru(tpy\text{-}pvp\text{-}Ph)_2]^{2+}$ (**5**)

	5					
	Ground State			Excited State		
	Trans-trans	*Trans-cis*	*Cis-cis*	*Trans-trans*	*Trans-cis*	*Cis-cis*
Ru1-N1	2.112	2.112	2.114	2.118	2.120	2.113
Ru1-N6	2.112	2.113	2.113	2.112	2.114	2.119
Ru1-N4	2.112	2.112	2.114	2.112	2.113	2.119
Ru1-N3	2.112	2.111	2.113	2.118	2.118	2.111
Ru1-N5	2.007	2.008	2.008	2.046	2.048	1.955
Ru1-N2	2.007	2.008	2.008	1.956	1.957	2.052
N1-Ru1-N6	92.2	92.5	92.4	92.3	92.4	92.5
N1-Ru1-N4	92.3	92.2	92.4	92.3	92.5	92.3
N6-Ru1-N4	156.7	156.7	156.5	154.4	154.3	158.5
N1-Ru1-N3	156.7	156.7	156.6	158.2	158.3	154.1
N6-Ru1-N3	92.4	92.2	92.3	92.3	92.4	92.6
N4-Ru1-N3	92.2	92.4	92.2	92.4	92.3	92.2
N1-Ru1-N5	101.7	101.7	101.7	100.7	101.0	103.0
N6-Ru1-N5	78.4	78.4	78.3	77.2	77.2	79.3
N4-Ru1-N5	78.3	78.2	78.2	77.2	77.2	79.2
N3-Ru1-N5	101.4	101.6	101.6	101.0	100.1	102.9
N1-Ru1-N2	78.3	78.4	78.2	79.1	79.1	77.0
N6-Ru1-N2	101.4	101.4	101.4	102.9	102.6	100.2
N4-Ru1-N2	101.7	101.8	101.9	102.5	102.9	101.3
N3-Ru1-N2	78.4	78.3	78.3	79.1	79.2	77.1
N5-Ru1-N2	179.7	179.8	179.7	179.7	179.8	179.4

Table S7. Selected MOs along with their Energies and Compositions in the Ground State for $[Ru(tpy\text{-}pvp\text{-}H)_2]^{2+}$ (**1**) in MeCN

MO	$[Ru(tpy\text{-}pvp\text{-}H)_2]^{2+}$ (**1**)															
	Energy/ev			% Compositions												
	Trans-trans	*Trans-cis*	*Cis-cis*	*Trans-trans*				*Trans-cis*				*Cis-cis*			
				Ru	tpy	Styryl-benz	Benz	Ru	tpy	Styry-benz	Benz	Ru	tpy	Styryl-benz	Benz
LUMO+5	-1.85	-1.75	-1.74	0.35	35.82	46.99	16.82	0.39	45.80	42.75	11.06	0.39	45.48	42.85	11.26
LUMO+4	-1.85	-1.86	-1.75	0.34	35.96	46.92	16.76	0.35	35.40	47.25	16.99	0.37	45.63	43.49	11.49
LUMO+3	-2.42	-2.42	-2.42	3.10	96.21	0.67	0.00	3.11	96.22	0.66	0.00	3.11	96.24	0.64	0.00
LUMO+2	-2.49	-2.50	-2.5	0.00	99.35	0.63	0.00	0.00	99.36	0.63	0.00	0.00	99.37	0.61	0.00
LUMO+1	-2.70	-2.69	-2.69	7.79	79.73	10.65	1.81	7.83	81.95	9.32	0.89	7.90	82.24	9.03	0.81
LUMO	-2.71	-2.70	-2.70	7.61	79.85	10.72	1.80	7.69	80.04	10.34	1.73	7.74	82.32	9.12	0.81
HOMO	-5.74	-5.75	-5.88	11.66	8.10	53.15	27.07	11.76	7.99	53.19	27.04	18.92	10.57	48.50	21.99
HOMO-1	-5.74	-5.88	-5.88	11.65	7.84	53.34	27.15	19.45	10.69	48.24	21.61	19.10	10.39	48.52	21.98
HOMO-2	-6.13	-6.14	-6.14	70.00	29.95	0.03	64.83	69.90	29.99	0.07	0.03	69.93	30.02	0.04	0.00
HOMO-3	-6.25	-6.25	-6.27	57.60	22.37	9.87	10.14	57.37	22.36	10.04	10.23	49.52	19.35	15.01	16.11
HOMO-4	-6.25	-6.27	-6.27	57.27	22.39	10.05	10.27	49.03	19.15	15.36	16.46	49.30	19.33	15.28	16.07
HOMO-5	-7.00	-6.97	-6.97	0.00	0.01	0.09	99.87	0.01	0.05	6.88	93.04	0.01	0.05	6.88	93.05

Table S8. Selected MOs along with their Energies and Compositions in the Ground State for $[Ru(tpy\text{-}pvp\text{-}Me)_2]^{2+}$ (**2**) in MeCN

MO	$[Ru(tpy\text{-}pvp\text{-}Me)_2]^{2+}$ (**2**)															
	Energy/ev			% Compositions												
	Trans-trans	*Trans-cis*	*Cis-cis*	*Trans-trans*				*Trans-cis*				*Cis-cis*			
				Ru	tpy	Styryl-benz	tolu	Ru	tpy	Styryl-benz	tolu	Ru	tpy	Styryl-benz	tolu
LUMO+5	-1.83	-1.73	-1.73	0.35	37.50	46.33	15.81	0.41	47.63	41.67	10.28	0.42	47.80	41.57	10.20
LUMO+4	-1.83	-1.83	-1.74	0.34	33.97	46.26	15.75	0.35	37.29	46.47	15.89	0.39	46.40	42.41	10.80
LUMO+3	-2.41	-2.41	-2.42	3.11	96.21	0.68	0.00	3.12	96.22	0.67	0.00	3.12	96.23	0.64	0.00
LUMO+2	-2.49	-2.49	-2.50	0.00	99.35	0.64	0.00	0.00	99.36	0.63	0.00	0.00	99.37	0.62	0.00
LUMO+1	-2.69	-2.69	-2.69	7.80	80.12	10.33	1.74	7.82	81.97	9.27	0.93	7.91	82.39	8.88	0.81
LUMO	-2.70	-2.70	-2.70	7.62	80.23	10.41	1.73	7.70	80.56	10.14	1.60	7.73	82.51	8.95	0.81
HOMO	-5.66	-5.66	-5.80	8.29	6.56	51.70	33.44	8.13	6.38	51.86	33.62	11.87	7.53	48.99	31.60
HOMO-1	-5.66	-5.79	-5.80	8.26	6.36	51.85	33.52	12.36	7.71	48.81	31.12	12.04	7.48	49.08	31.39
HOMO-2	-6.13	-6.13	-6.14	70.01	29.95	0.03	0.00	69.86	29.97	0.08	0.07	69.93	30.03	0.03	0.00
HOMO-3	-6.22	-6.22	-6.22	60.31	23.35	6.82	9.51	59.72	23.22	6.99	10.06	55.48	21.51	8.59	14.41
HOMO-4	-6.22	-6.22	-6.23	59.93	23.44	6.95	9.66	55.65	21.63	8.58	14.15	55.35	21.64	8.72	14.27
HOMO-5	-6.97	-6.92	-6.92	0.00	0.00	0.06	99.94	0.11	0.17	6.05	93.66	0.12	0.17	6.15	93.55

Table S9. Selected MOs along with their Energies and Compositions in the Ground State for $[Ru(tpy\text{-}pvp\text{-}Cl)_2]^{2+}$ (**3**) in MeCN

MO	$[Ru(tpy\text{-}pvp\text{-}Cl)_2]^{2+}$ (**3**)															
	Energy/ev			% Compositions												
	Trans-trans	*Trans-cis*	*Cis-cis*	*Trans-trans*				*Trans-cis*				*Cis-cis*			
				Ru	tpy	Styryl-benz	Cl-benz	Ru	tpy	Styryl-benz	Cl-benz	Ru	tpy	Styryl-benz	Cl-benz
LUMO+5	-1.92	-1.80	-1.8	0.39	31.57	46.99	21.04	0.34	38.63	45.11	15.92	0.33	38.47	45.29	15.88
LUMO+4	-1.93	-1.93	-1.81	0.37	31.75	46.91	20.95	0.38	31.22	47.19	21.22	0.31	37.34	45.76	16.57
LUMO+3	-2.42	-2.43	-2.43	3.09	96.22	0.67	0.00	3.11	96.22	0.67	0.00	3.10	96.23	0.65	0.00
LUMO+2	-2.5	-2.50	-2.51	0.00	99.35	0.63	0.00	0.00	99.36	0.63	0.00	0.00	99.36	0.62	0.00
LUMO+1	-2.71	-2.71	-2.7	7.74	78.45	11.52	2.28	7.81	81.08	10.01	1.10	7.88	81.49	9.60	1.01
LUMO	-2.72	-2.72	-2.71	7.56	78.59	11.57	2.26	7.63	78.79	11.38	2.19	7.72	11.94	9.68	0.99
HOMO	-5.79	-5.80	-5.92	13.32	8.66	50.79	27.21	13.47	8.56	50.80	27.16	22.82	11.94	44.73	20.49
HOMO-1	-5.79	-5.92	-5.92	13.31	8.38	50.99	27.30	23.15	12.03	44.42	20.40	22.64	11.69	44.64	21.02
HOMO-2	-6.14	-6.14	-6.14	70.00	29.95	0.03	0.00	69.91	29.98	0.07	0.03	69.93	30.02	0.03	0.00
HOMO-3	-6.26	-6.26	-6.29	55.84	21.72	10.42	12.00	55.57	21.67	10.63	12.12	45.69	17.97	16.78	19.53
HOMO-4	-6.26	-6.29	-6.29	55.50	21.72	10.61	12.16	45.17	17.72	17.04	20.07	45.38	17.84	16.92	19.84
HOMO-5	-7.23	-7.20	-6.92	0.00	93.71	6.25	0.02	3.57	10.33	42.85	43.25	3.54	8.54	41.63	46.27

Table S10. Selected MOs along with their Energies and Compositions in the Ground State for $[Ru(tpy\text{-}pvp\text{-}NO_2)_2]^{2+}$ (**4**) in MeCN

MO	$[Ru(tpy\text{-}pvp\text{-}Cl)_2]^{2+}$ (**3**)															
	Energy/ev			% Compositions												
	Trans-trans	*Trans-cis*	*Cis-cis*	*Trans-trans*				*Trans-cis*				*Cis-cis*			
				Ru	tpy	Styryl-benz	Cl-benz	Ru	tpy	Styryl-benz	Cl-benz	Ru	tpy	Styryl-benz	Cl-benz
LUMO+5	-1.92	-1.80	-1.8	0.39	31.57	46.99	21.04	0.34	38.63	45.11	15.92	0.33	38.47	45.29	15.88
LUMO+4	-1.93	-1.93	-1.81	0.37	31.75	46.91	20.95	0.38	31.22	47.19	21.22	0.31	37.34	45.76	16.57
LUMO+3	-2.42	-2.43	-2.43	3.09	96.22	0.67	0.00	3.11	96.22	0.67	0.00	3.10	96.23	0.65	0.00
LUMO+2	-2.5	-2.50	-2.51	0.00	99.35	0.63	0.00	0.00	99.36	0.63	0.00	0.00	99.36	0.62	0.00
LUMO+1	-2.71	-2.71	-2.7	7.74	78.45	11.52	2.28	7.81	81.08	10.01	1.10	7.88	81.49	9.60	1.01
LUMO	-2.72	-2.72	-2.71	7.56	78.59	11.57	2.26	7.63	78.79	11.38	2.19	7.72	11.94	9.68	0.99
HOMO	-5.79	-5.80	-5.92	13.32	8.66	50.79	27.21	13.47	8.56	50.80	27.16	22.82	11.94	44.73	20.49
HOMO-1	-5.79	-5.92	-5.92	13.31	8.38	50.99	27.30	23.15	12.03	44.42	20.40	22.64	11.69	44.64	21.02
HOMO-2	-6.14	-6.14	-6.14	70.00	29.95	0.03	0.00	69.91	29.98	0.07	0.03	69.93	30.02	0.03	0.00
HOMO-3	-6.26	-6.26	-6.29	55.84	21.72	10.42	12.00	55.57	21.67	10.63	12.12	45.69	17.97	16.78	19.53
HOMO-4	-6.26	-6.29	-6.23	55.50	21.72	10.61	12.16	45.17	17.72	17.04	20.07	45.38	17.84	16.92	19.84
HOMO-5	-7.23	-7.20	-6.92	0.00	93.71	6.25	0.02	3.57	10.33	42.85	43.25	3.54	8.54	41.63	46.27

Table S11. Selected MOs along with their Energies and Compositions in the Ground State for $[Ru(tpy\text{-}pvp\text{-}Ph)_2]^{2+}$ (**5**) in MeCN

MO	$[Ru(tpy\text{-}pvp\text{-}Ph)_2]^{2+}$ (**5**)															
	Energy/ev			% Compositions												
	Trans-trans	*Trans-cis*	*Cis-cis*	*Trans-trans*				*Trans-cis*				*Cis-cis*			
				Ru	tpy	Styryl-benz	Biphen	Ru	tpy	Styryl-benz	Biphen	Ru	tpy	Styryl-benz	Biphen
LUMO+5	-1.85	-1.82	-1.74	0.35	35.82	46.99	16.82	0.32	34.62	42.83	22.23	0.39	45.48	42.85	11.26
LUMO+4	-1.85	-1.93	-1.75	0.34	35.96	46.92	16.76	0.37	29.59	43.87	26.17	0.37	45.63	43.49	11.49
LUMO+3	-2.42	-2.42	-2.42	3.10	96.21	0.67	0.00	3.11	96.21	0.68	0.00	3.11	96.24	0.64	0.00
LUMO+2	-2.49	-2.50	-2.5	0.00	99.35	0.63	0.00	0.00	99.36	0.65	0.00	0.00	99.37	0.61	0.00
LUMO+1	-2.70	-2.70	-2.69	7.79	79.73	10.65	1.81	7.78	80.93	9.99	1.29	7.90	82.24	9.03	0.81
LUMO	-2.71	-2.71	-2.70	7.61	79.85	10.72	1.80	7.62	78.70	11.23	2.44	7.74	82.32	9.12	0.81
HOMO	-5.74	-5.63	-5.88	11.66	8.10	53.15	27.07	6.31	5.21	45.00	43.47	18.92	10.57	48.50	21.99
HOMO-1	-5.74	-5.76	-5.88	11.65	7.84	53.34	27.15	8.61	5.75	41.63	44.01	19.10	10.39	48.52	21.98
HOMO-2	-6.13	-6.14	-6.14	70.00	29.95	0.03	64.83	69.92	29.96	0.05	0.07	69.93	30.02	0.04	0.00
HOMO-3	-6.25	-6.18	-6.27	57.60	22.37	9.87	10.14	55.20	21.62	4.97	18.21	49.52	19.35	15.01	16.11
HOMO-4	-6.25	-6.19	-6.27	57.27	22.39	10.05	10.27	58.80	23.01	4.51	13.68	49.30	19.33	15.28	16.07
HOMO-5	-7.00	-6.79	-6.97	0.00	0.01	0.09	99.87	6.94	5.85	37.08	50.13	0.01	0.05	6.88	93.05

Table S12. Selected UV-vis Energy Transitions at the TD-DFT/B3LYP Level of [Ru(tpy-pvp-H)$_2$]$^{2+}$ (**1**) in MeCN

Excited state	λ_{cal}/nm	Oscillator strength(f)	λ_{expt}/nm	Key transitions	Character
Trans-trans [Ru(tpy-pvp-H)$_2$]$^{2+}$ (**1**)					
S_4	490	1.43	497	H-1→L+1 (43%), H→L(39%), H-4→L (7%), H-3→L+1 (9%)	MLCT,ILCT
S23	355	2.06	332	H-1→L+4 (46%), H→L+5(46%)	ILCT
S_{41}	314	0.19	312	H-8→L (11%), H-7→L+1 (36%), H-2→L+5 (27%), H-10→L(4%), H-2→L+7 (9%)	ILCT ,π-π*
S_{81}	278	0.23	289	H-10→L+2 (19%), H-8→L+2(11%), H-7→L+3 (38%),H-9→L+3 (4%), H-1→L+11 (8%), H→L+10 (8%)	π-π*, ILCT
Trans-cis [Ru(tpy-pvp-H)$_2$]$^{2+}$ (**1**)					
S_5	484	1.13	493	H-1→L+1 (23%), H→L (51%), H-4→L+1 (6%), H-3→L (8%), H→L+1 (4%)	MLCT,ILCT
S22	349	1.15	335	H→L+4 (92%), H-3→L+4(3%)	ILCT
S_{41}	310	0.26	310	H-8→L+1 (19%), H-7→L+1 (34%), H-2→L+5 (24%) H-9→L+1 (5%)	ILCT ,π-π*
S_{80}	278	0.30	289	H-10->L+2 (14%), H-9->L+2 (14%), H-8->L+3 (17%), H-7->L+3 (25%), , HOMO->L+11 (6%)	π-π*, ILCT
Cis-cis [Ru(tpy-pvp-H)$_2$]$^{2+}$ (**1**)					
S_5	477	0.77	493	H-1→L+1 (41%), H→L (38%), H-4→L (5%), H-3→L+1 (6%)	MLCT,ILCT
S22	340	0.89	335	H-1→L+4 (21%), H-1→L+5 (11%), H→L+4 (53%), H→L+5 (7%)	ILCT
S_{40}	312	0.26	310	H-7→L+1 (43%), H-2→L+5 (24%), H-7→L (7%), H-5->L+1 (5%)	ILCT ,π-π*
S_{78}	280	0.22	289	H-11→L+2 (16%), H-7→L+3 (30%),H-12→L+2 (9%), H-11→L+3 (9%), H-10→L+2 (8%), H-8→L+2 (8%)	π-π*, ILCT

Table S13. Selected UV-vis Energy Transitions at the TD-DFT/B3LYP Level of [Ru(tpy-pvp-Me)$_2$]$^{2+}$ (**2**) in MeCN

Excited state	λ_{cal}/nm	Oscillator strength(f)	λ_{expt}/nm	Key transitions	Character
Trans-trans [Ru(tpy-pvp-Me)$_2$]$^{2+}$ (**2**)					
S_3	497	1.55	500	H-1→L+1 (46%), H→L (38%), H-4→L (5%), H-3→L+1 (9%)	MLCT,ILCT
S_{22}	360	2.25	333	H-1→L+4 (47%), H→L+5 (47%)	ILCT
S_{42}	310	0.23	313	H-7→L+1 (40%), H-2→L+5 (30%), H-12→L (4%), H-10 →L (7%), H-2→L+7 (6%)	ILCT ,π-π*
S_{82}	279	0.26	289	H-12→L+2 (17%), H-7→L+3 (29%), H-1→L+11 (14%), H→L+10 (15%), H-10→L+2 (5%)	π-π*, ILCT
Trans-cis [Ru(tpy-pvp-Me)$_2$]$^{2+}$ (**2**)					
S_3	492	1.2	492	H-1→L+1 (18%), H→L (53%), H-3→L (5%), H→L+1 (8%)	MLCT,ILCT
S_{23}	345	1.26	332	H-1→L+5 (92%)	ILCT
S_{42}	311	0.23	312	H-8→L+1 (41%), H-7→L+1 (12%), H-2→L+5 (22%), H-8→L (5%)	ILCT ,π-π*
S_{83}	278	0.33	288	H-12→L+2 (19%), H-8→L+3 (36%), H→L+11 (13%), H-10→L+2 (8%)	π-π* , ILCT
Cis-cis [Ru(tpy-pvp-Me)$_2$]$^{2+}$ (**2**)					
S_5	481	0.94	492	H-3→L+1 (10%), H-1→L+1 (30%), H→L (28%), H→L+1 (10%), H-4→L (8%), H-1→L (9%)	MLCT,ILCT
S_{22}	346	1.09	332	H-1→L+5 (24%), H→L+4 (59%), H-1→L+4 (6%)	ILCT
S_{41}	311	0.24	312	H-9→L (55%), H-2→L+4 (16%) H-7→L (3%), H-2→L+5 (7%),	ILCT ,π-π*
S_{114}	246	0.15	288	H-12→L+2 (21%), H-10→L+2 (11%), H-9→L+3 (44%)	π-π* , ILCT

Table S14. Selected UV-vis Energy Transitions at the TD-DFT/B3LYP Level of [Ru(tpy-pvp-Cl)$_2$]$^{2+}$ (**3**) in MeCN

Excited state	λ_{cal}/nm	Oscillator strength(f)	λ_{expt}/nm	Key transitions	Character
Trans-trans [Ru(tpy-pvp-Cl)$_2$]$^{2+}$ (**3**)					
S_5	487	1.55	500	H-1→L+1 (42%), H→L(37%), H-4→L (7%), H-3→L+1 (9%)	MLCT,ILCT
S_{22}	358	2.25	333	H-1→L+4 (46%), H→L+5 (47%)	ILCT
S_{38}	316	0.23	313	H-6→LUMO (12%), H-5→L+1 (29%), H-2→L+5 (19%), H-2→L+7 (13%), H-1→L+9 (12%), H-3->L+9 (7%)	ILCT ,π-π*
S_{105}	251	0.322	245	H-12→L+5 (15%), H-11→L+4 (15%), H-4→L+10 (17%), H-3→L+11 (18%) H-14→LUMO (7%), H-13→L+1 (8%), H-10→L+5 (5%), H-9→L+4 (5%)	π-π*, ILCT
Trans-cis [Ru(tpy-pvp-Cl)$_2$]$^{2+}$ (**3**)					
S_5	482	1.18	492	H-1→L+1 (26%), H→L (50%), H-4→L+1 (6%), H-3→L (9%)	MLCT,ILCT
S_{23}	342	1.20	333	H-1→L+5 (91%)	ILCT
S_{41}	312	0.13	310	H-7→L+1 (11%), H-6→L+1 (15%), H-4→L+9 (11%), H-2→L+5 (17%), H-1→L+9 (25%)	ILCT ,π-π*
S_{113}	246	0.19	247	H-14→L+2 (30%), H-13→L+2 (40%), H-13→L+3 (8%)	π-π* , ILCT
Cis-cis [Ru(tpy-pvp-Cl)$_2$]$^{2+}$ (**3**)					
S_5	474	0.87	492	H-1→L (11%), H-1→L+1 (28%), H→L (28%), H→L+1 (13%), H-4→L(7%), H-3→L+1 (8%)	MLCT,ILCT
S_{22}	343	1.07	333	H-1→L+4 (46%), H→L+5 (46%)	ILCT
S_{38}	311	0.22	310	H-9→L+1 (16%), H-7→L+1 (11%), H-2→L+4 (13%), H-1→L+9 (20%), H-3→L+9 (9%), H-2→L+5 (7%)	ILCT ,π-π*
S_{109}	246	0.18	247	H-14→L+2 (32%), H-13→L+2 (41%), H-13→L+3 (9%), H-10→L+4 (3%), H-9→L+4 (3%)	π-π* , ILCT

Table S15. Selected UV-vis Energy Transitions at the TD-DFT/B3LYP Level of $[Ru(tpy\text{-}pvp\text{-}NO_2)_2]^{2+}$ (**4**) in MeCN

Excited state	λ_{cal}/nm	Oscillator strength(f)	λ_{expt}/nm	Key transitions	Character
Trans-trans $[Ru(tpy\text{-}pvp\text{-}NO_2)_2]^{2+}$ (**4**)					
S_5	487	2.09	500	H-1→L+1 (38%), H→L (36%), H-1→L+3 (9%), H→L+2 (7%)	MLCT,ILCT
S_{11}	428	0.97	371	H-2→L+4 (60%) H-4→L (5%), H-1→L+1 (6%), H-1->L+3 (7%), H→L (6%), H→L+2 (8%)	MLCT,ILCT
S_{55}	308	0.37	313	H-1→L+10 (27%), H→L+9 (29%), H-10→L (6%), H-9→L+1 (6%), H-1→L+6 (6%), H→L+7 (7%)	ILCT ,π-π*
S_{64}	292	0.15	286	H-4→L+7 (35%), H-3→L+6 (37%), H-6→L+4 (6%), H-1→L+10 (6%), H→L+9 (5%)	π-π* , ILCT
trans-cis $[Ru(tpy\text{-}pvp\text{-}NO_2)_2]^{2+}$ (**4**)					
S_5	482	1.52	493	H-1→L+1 (23%), H→L (49%), H→L+3 (10%), H-1→L+2 (9%)	MLCT,ILCT
S_{10}	427	0.55	380	H-2→L+4 (43%), H-1→L+5 (16%), H→L (11%), H→L+3 (12%), H-3→L (7%)	MLCT,ILCT
S_{37}	329	0.28	336	H→L+6 (66%), H-3→L+9 (4%), H-1→L+7 (5%), H→L+9 (9%)	ILCT
S_{51}	310	0.25	313	H-6→L (39%), H-2→L+6 (24%), H-8→L (8%), H-7→->L (5%), H-6→L+3 (9%)	ILCT ,π-π*
S_{82}	282	0.34	288	H-11→L+1 (30%), H-9→L+1 (15%), H-4→L+7 (14%), H-2→L+11 (11%), H-12→L (5%), H-5→L+5 (5%)	π-π* , ILCT
Cis-cis $[Ru(tpy\text{-}pvp\text{-}NO_2)_2]^{2+}$ (**4**)					
S_5	475	0.97	493	H-1→L (26%), H→L+1 (28%), H-1→L+1 (6%), H-1→L+2 (6%), H-1→L+3 (7%), H→L (6%), H→L+2 (6%), H→L+3 (7%)	MLCT,ILCT
S_{19}	426	0.44	380	H-2→L+4 (71%), H-1→L (5%), H→L+1 (5%)	MLCT,ILCT
S_{37}	328	0.31	336	H-1→L+7 (10%), H→L+6 (65%), H→L+10 (7%)	ILCT
S_{53}	306	0.36	313	H-1→L+9 (20%), H→L+10 (40%), H-10→L+1 (5%), H→L+6 (5%)	ILCT ,π-π*
S_{80}	283	0.69	288	H-12→L (21%), H-11→L+1 (20%), H-10→L (5%), H-10→L+1 (5%), H-9→L (5%), H-9→L+1 (5%), H-5->L+5 (6%)	π-π* , ILCT

Table S16. Selected UV-vis Energy Transitions at the TD-DFT/B3LYP Level of [Ru(tpy-pvp-Ph)$_2$]$^{2+}$ (**5**) in MeCN

Excited state	λ_{cal}/nm	Oscillator strength(f)	λ_{expt}/nm	Key transitions	Character
Trans-trans [Ru(tpy-pvp-Ph)$_2$]$^{2+}$ (**5**)					
S_2	501	1.88	501	H-4→L+1 (10%), H-1→L+1 (48%), H→L (36%), H-3→L (5%)	MLCT,ILCT
S_{21}	373	2.78	358	H-1→L+4 (48%), H→L+5 (48%)	ILCT
S_{61}	303	0.32	313	H-14→L (20%), H-12→L (15%), H-2→L+7 (45%)	π-π* ,ILCT ILCT, π-π*
Trans-cis [Ru(tpy-pvp-Ph)$_2$]$^{2+}$ (**5**)					
S_2	496	1.44	492	H-1→L+1 (18%), H→L (61%), H-4→L (8%), H-3→L+1 (7%)	MLCT,ILCT
S_{21}	368	1.32	333	H→L+4 (95%)	ILCT
S_{62}	303	0.32	308	H-14→L (13%), H-12→LUMO (15%), H-2→L+7 (44%) H-13→LUMO (8%)	ILCT, π-π*
S_{94}	279	0.34	288	H-14→L+2 (10%), H-11→L+3 (29%), H-6→L+4 (18%), H-13→L+3 (5%), H-12→L+2 (9%)	π-π* , ILCT
Cis-cis [Ru(tpy-pvp-Ph)$_2$]$^{2+}$ (**5**)					
S_5	482	0.91	492	H-4→L (10%), H-3→L+1 (11%), H-1→L (12%), H-1→L+1 (23%), H→L (23%), H→L+1 (13%)	MLCT,ILCT
S_{22}	354	1.32	333	H-1→L+4 (47%), H→L+5 (43%)	ILCT
S_{93}	280	0.44	288	H-14→L+2 (10%), H-12→L+2 (12%), H-11→L+3 (22%), H-9→L+3 (23%), H-1→L+11 (6%)	π-π* , ILCT

Table S17. Electrochemical Data for **1-5** in MeCN

Compounds	Oxidation[b] $E_{1/2}$(ox) / V	Reduction [c] $E_{1/2}$(red) / V
1	1.29	-1.15, -1.39
2	1.28	-1.16,-1.40
3	1.28	-1.03,-1.37
4	1.29	-0.91,-1.24,-1.47
5	1.28	-1.15,-1.35

[a]All the potentials are referenced against Ag/AgCl electrode with $E_{1/2}$ = 0.36 V for Fc/Fc^+ couple. [b]Reversible electron transfer process with a Pt working electrode. [c]$E_{1/2}$ values obtained from SWV using glassy carbon electrode.

Figures for Supporting Information

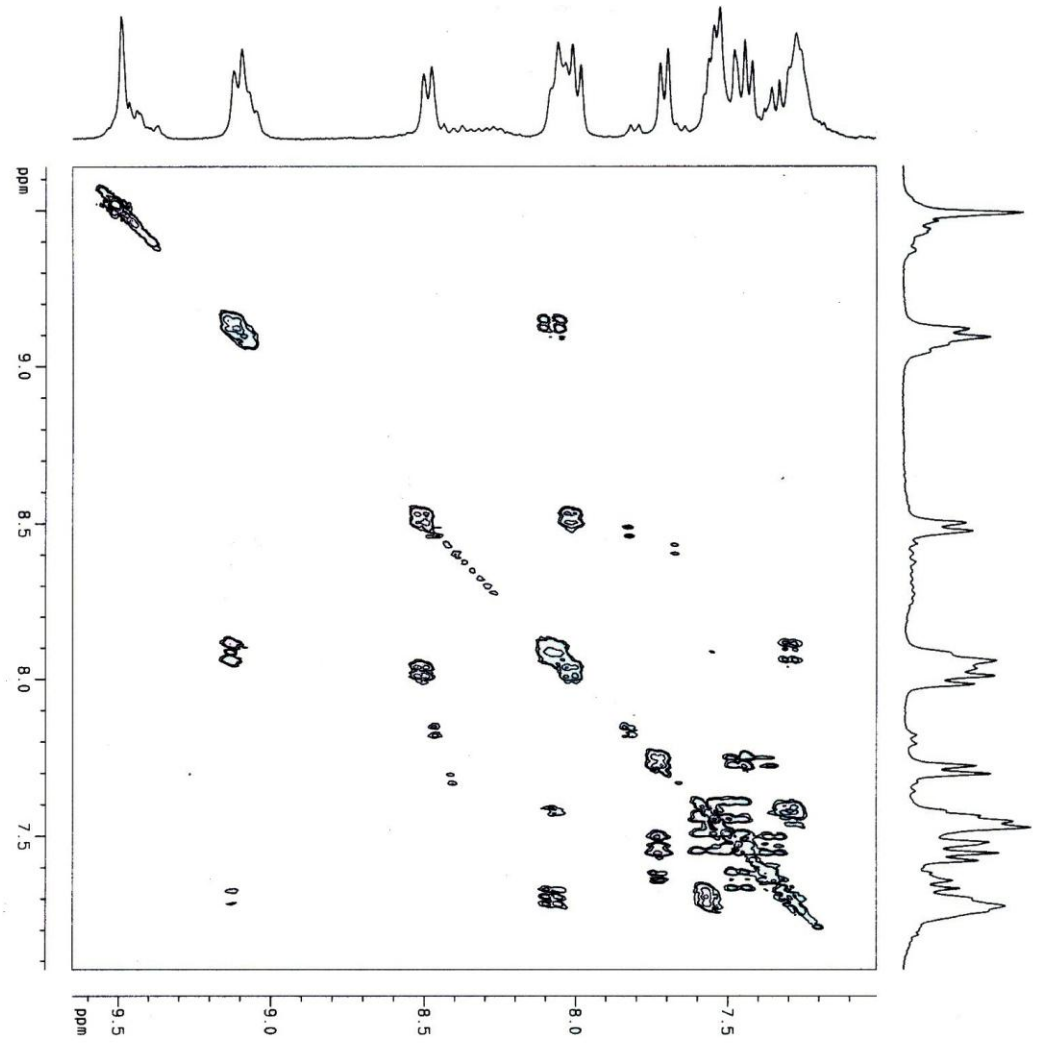

Figure S1. {^{1}H–^{1}H} COSY NMR spectrum of **1** in DMSO-d_6.

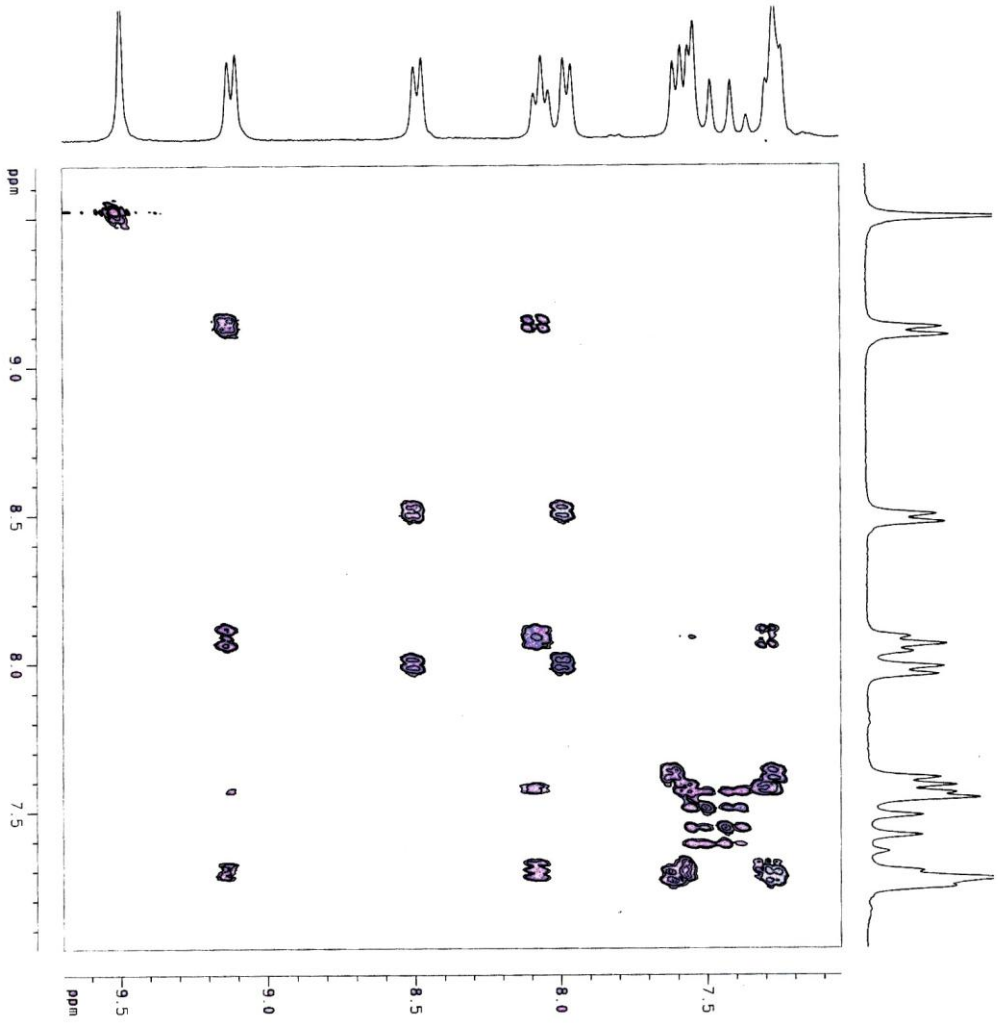

Figure S2. {^{1}H–^{1}H} COSY NMR spectrum of **2** in DMSO-d_6.

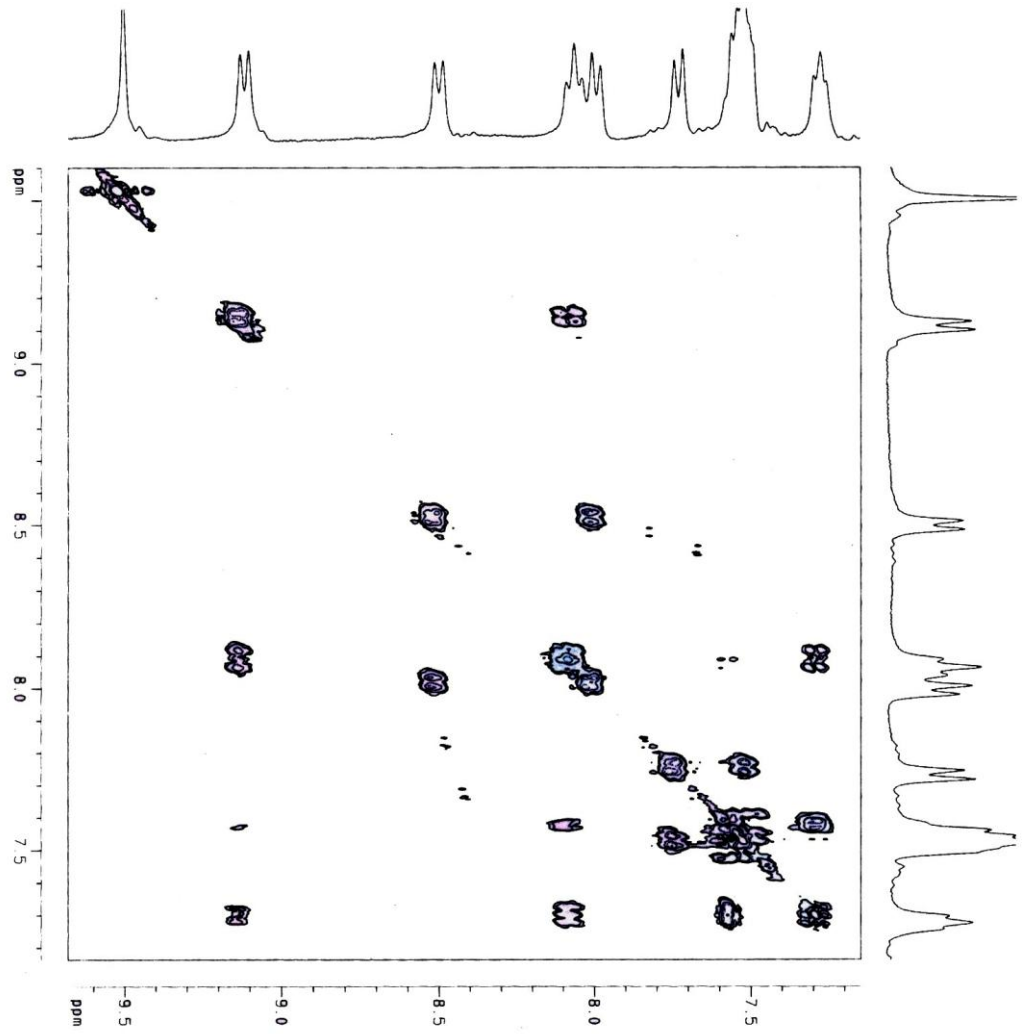

Figure S3. {^{1}H–^{1}H} COSY NMR spectrum of **3** in DMSO-d_6.

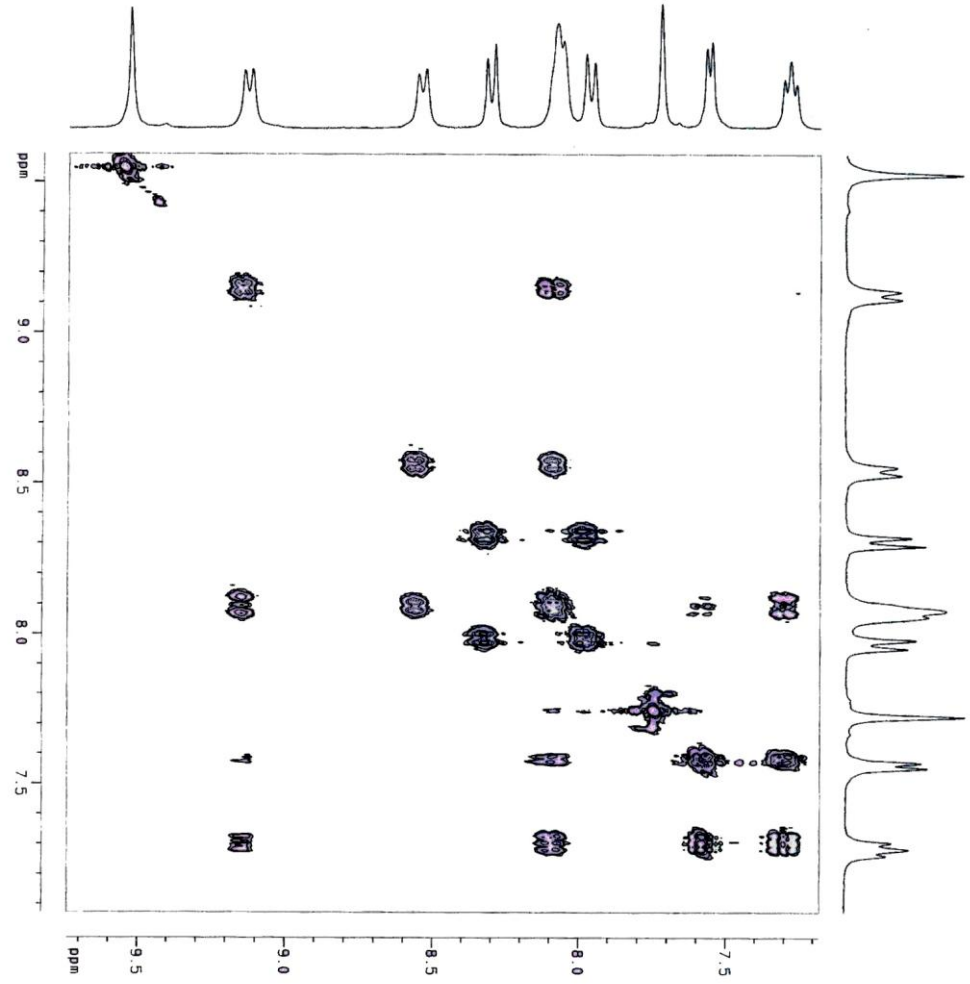

Figure S4. {^{1}H–^{1}H} COSY NMR spectrum of **4** in DMSO-d_6.

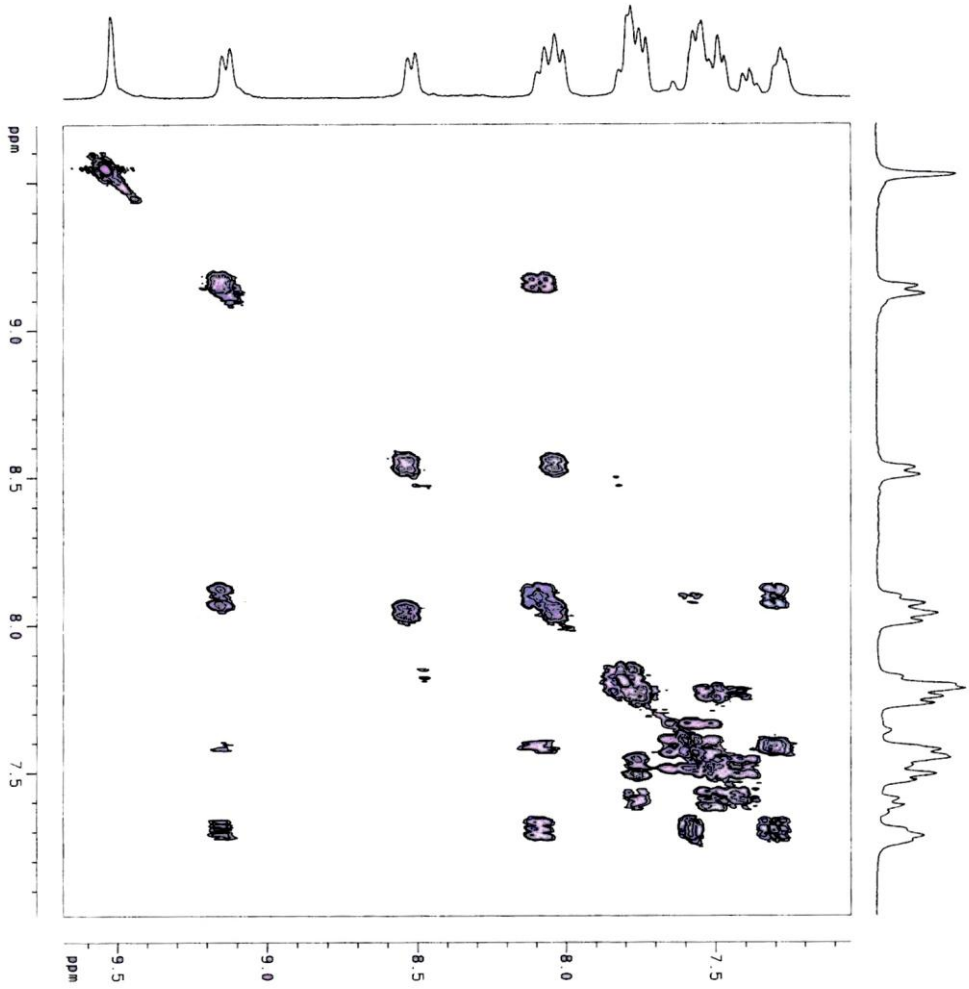

Figure S5. {^{1}H–^{1}H} COSY NMR spectrum of **5** in DMSO-d_6.

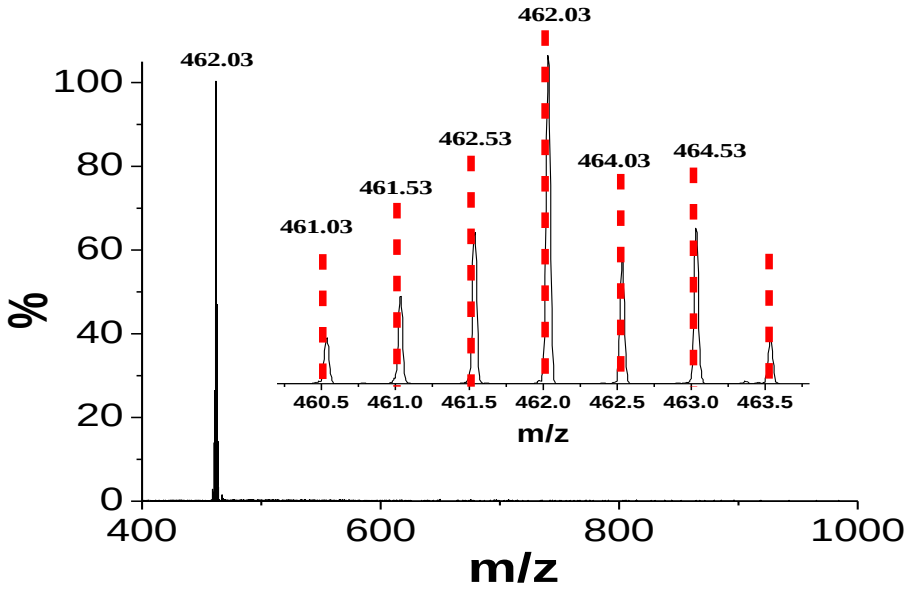

Figure S6. ESI (positive) mass spectrum for the complex cation of **1** $[(Ru(tpy\text{-}pvp\text{-}H)_2]^{2+}$ (m/z = 462.03) in MeCN showing both observed and simulated isotopic distribution patterns.

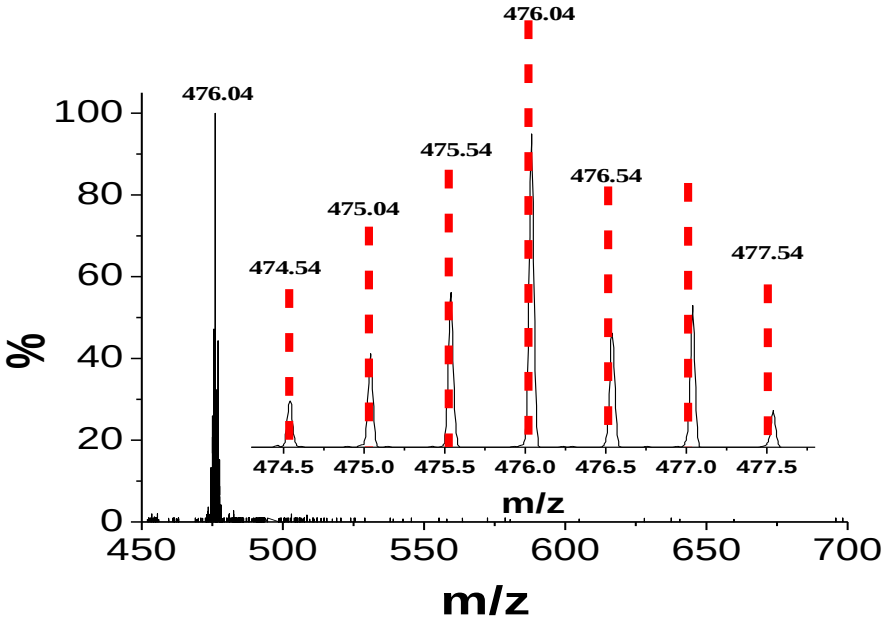

Figure S7. ESI (positive) mass spectrum for the complex cation of **2** $[(Ru(tpy\text{-}pvp\text{-}Me)_2]^{2+}$ (m/z = 476.04) in MeCN showing both observed and simulated isotopic distribution patterns.

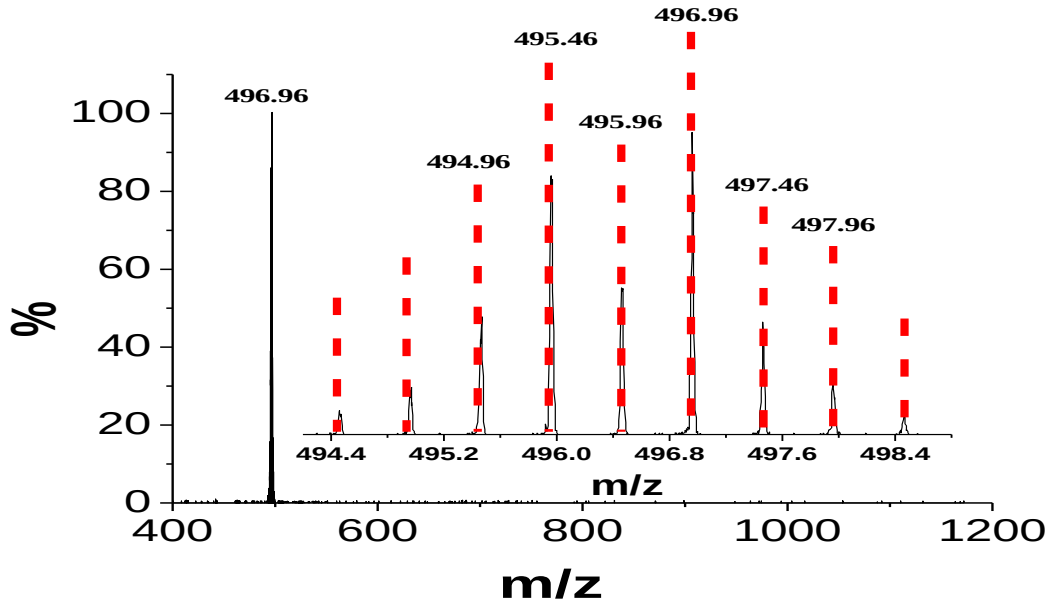

Figure S8. ESI (positive) mass spectrum for the complex cation of **3** $[(Ru(tpy\text{-}pvp\text{-}Cl)_2]^{2+}$ (m/z = 496.96) in MeCN showing both observed and simulated isotopic distribution patterns.

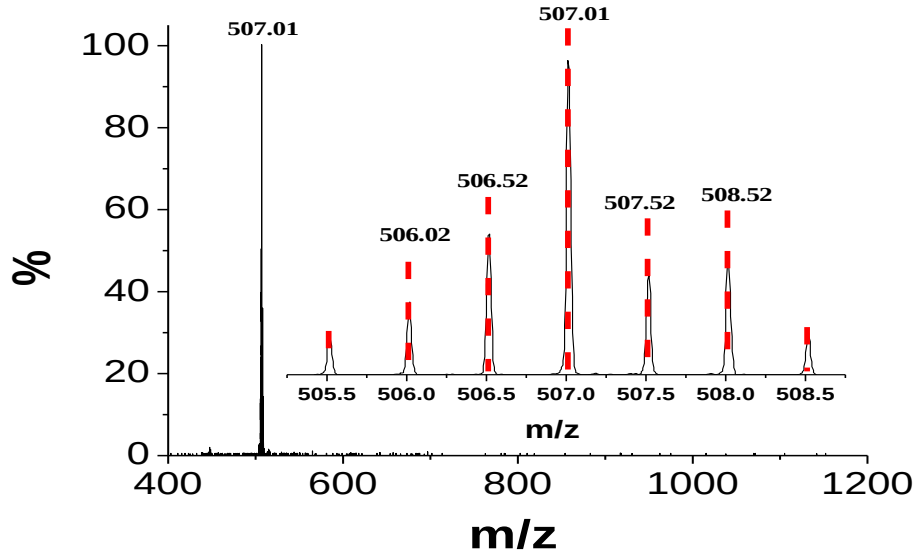

Figure S9. ESI (positive) mass spectrum for the complex cation of **4** $[(Ru(tpy\text{-}pvp\text{-}NO_2)_2]^{2+}$ (m/z = 507.01) in MeCN showing both observed and simulated isotopic distribution patterns.

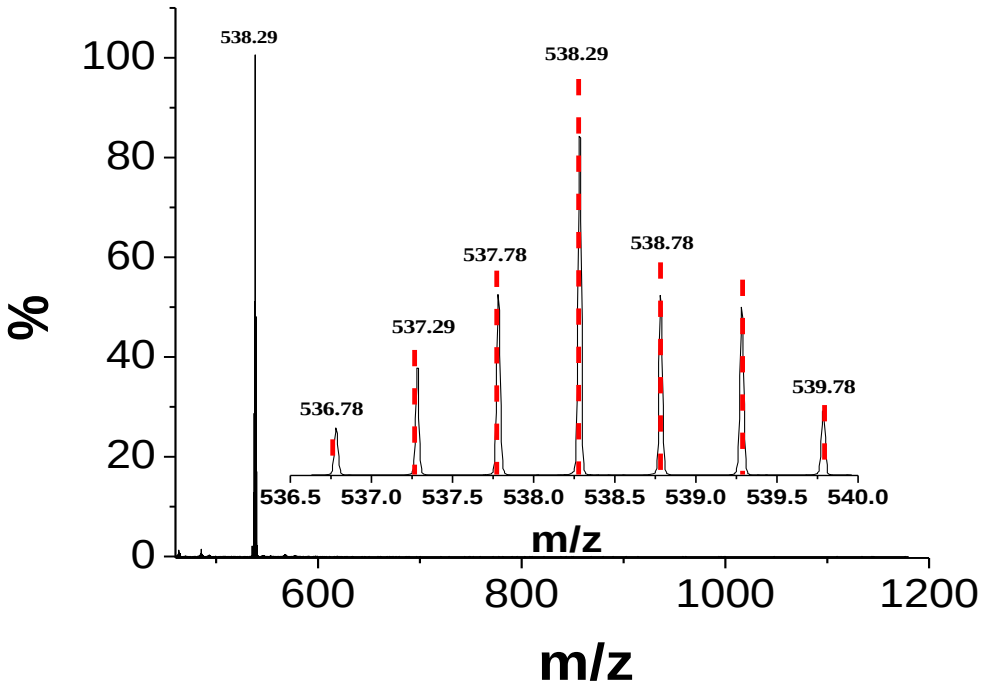

Figure S10. ESI (positive) mass spectrum for the complex cation of **5** $[(Ru(tpy\text{-}pvp\text{-}Ph)_2]^{2+}$ (m/z = 538.29) in MeCN showing both observed and simulated isotopic distribution patterns.

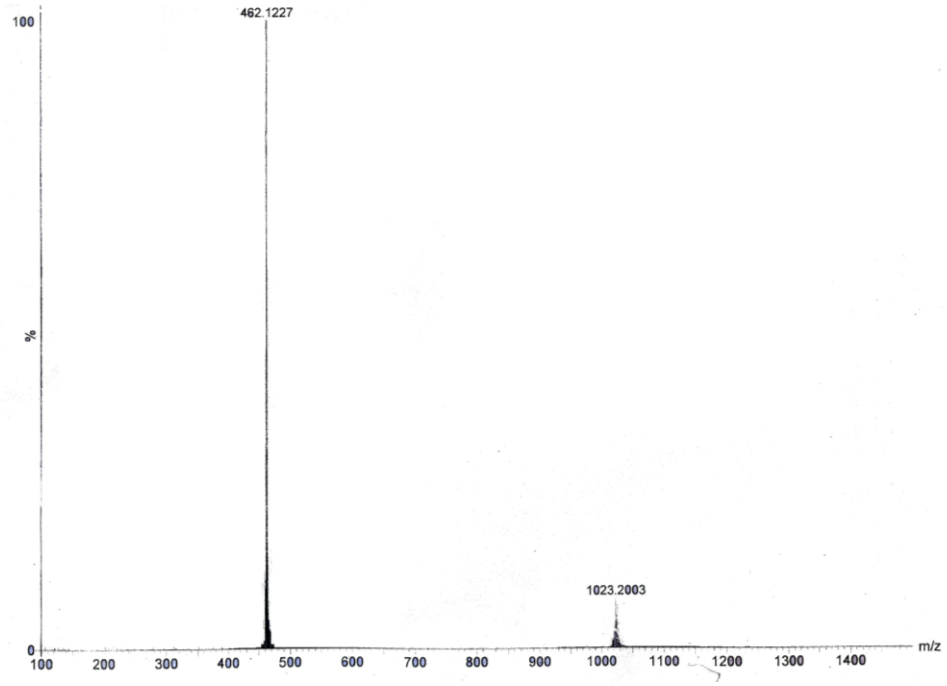

Figure S11. Scan copy of ESI (positive) mass spectrum for **1** in MeCN.

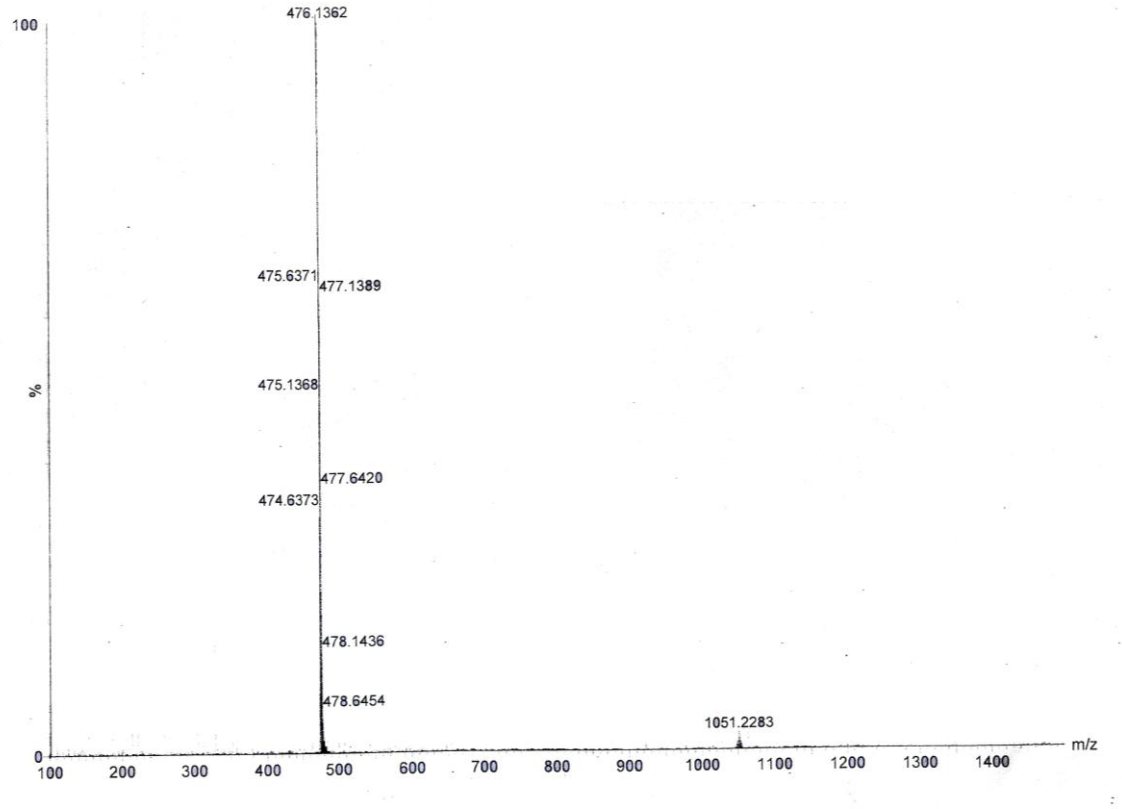

Figure S12. Scan copy of ESI (positive) mass spectrum for **2** in MeCN.

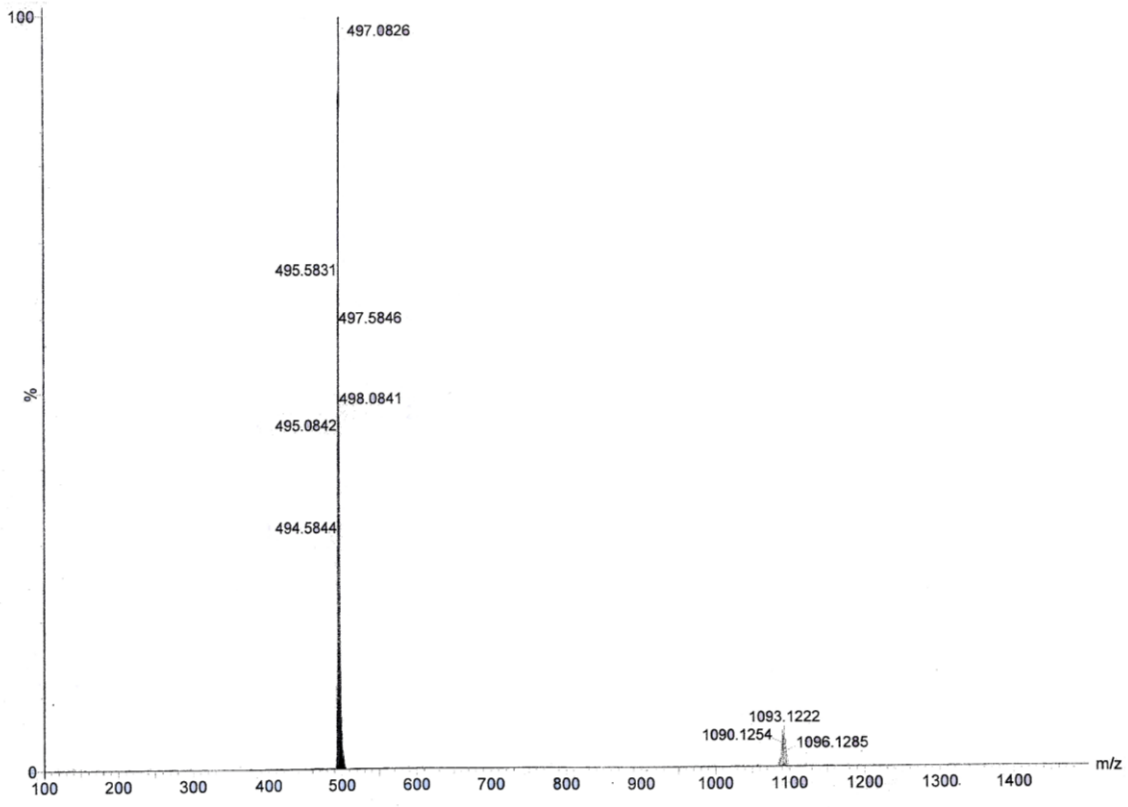

Figure S13. Scan copy of ESI (positive) mass spectrum for **3** in MeCN.

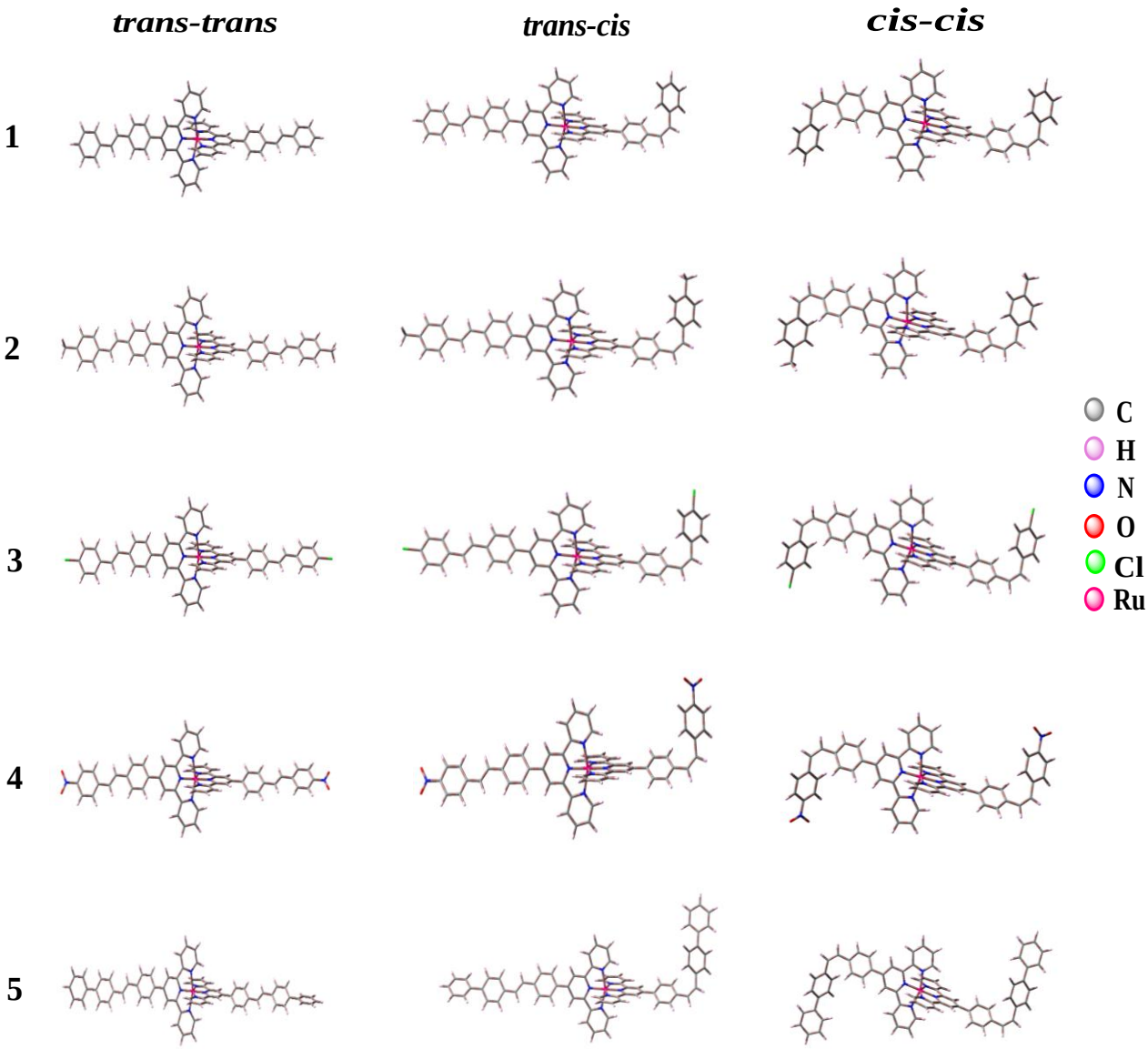

Figure S14. Ground state optimized geometries of *trans-trans*, *trans-cis* and *cis-cis* forms of **1-5** in MeCN.

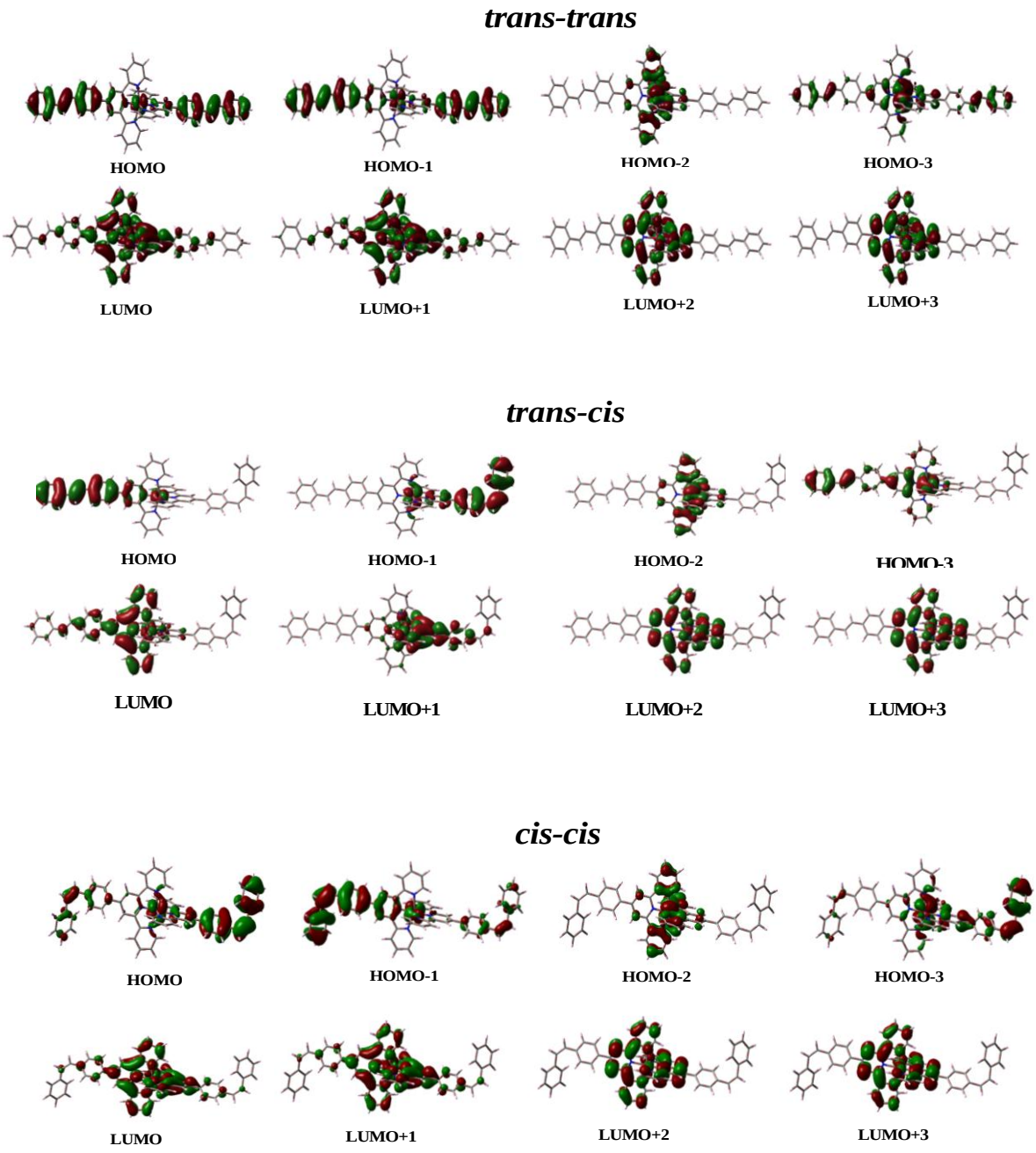

Figure S15. Schematic drawings of the selective frontier molecular orbitals of *trans-trans*, *trans-cis* and *cis-cis* form of $[(Ru(tpy\text{-}pvp\text{-}H)_2]^{2+}$ (**1**) in MeCN.

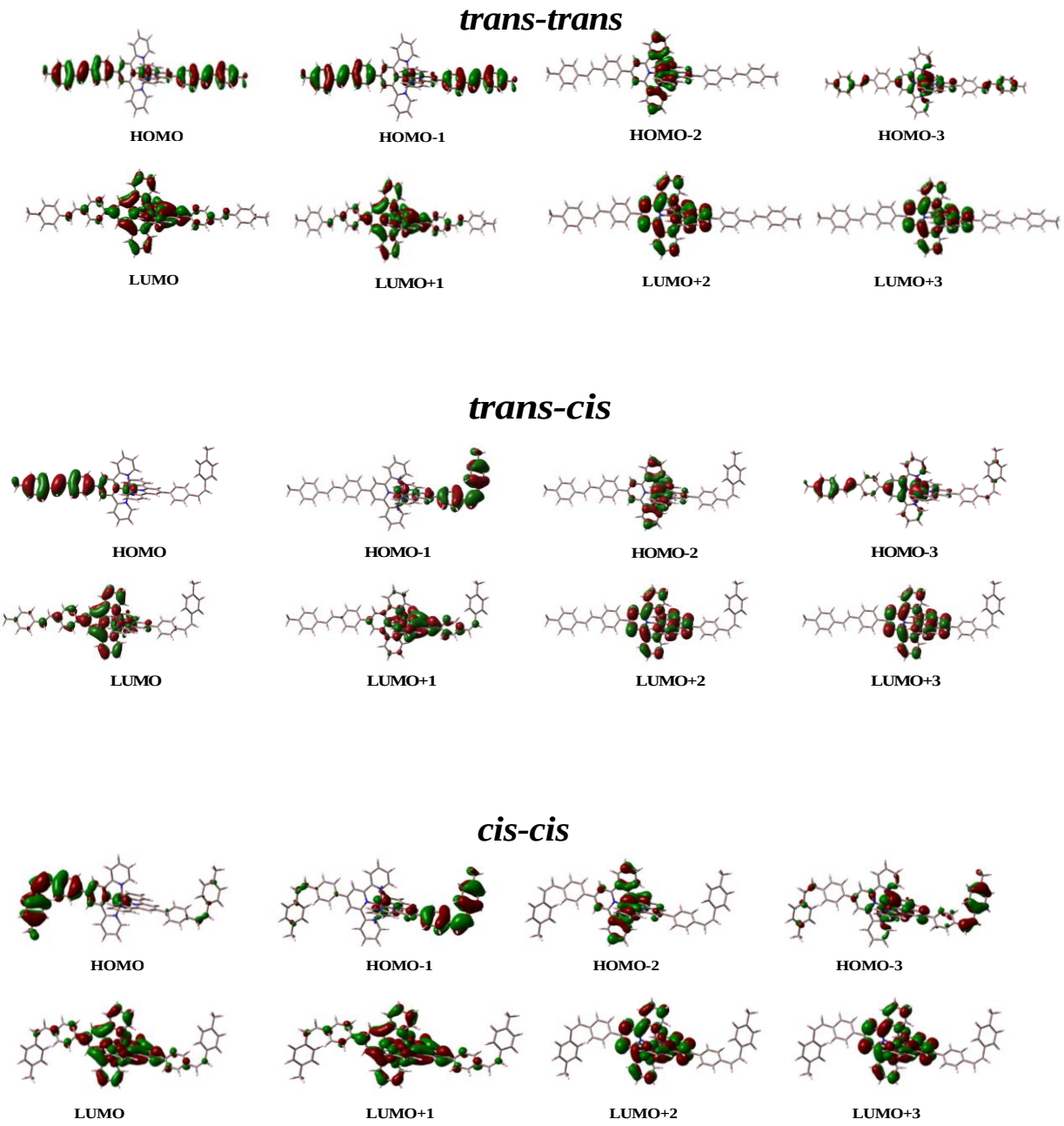

Figure S16. Schematic drawings of the selective frontier molecular orbitals of *trans-trans*, *trans-cis* and *cis-cis* form of $[(Ru(tpy\text{-}pvp\text{-}Me)_2]^{2+}$ (**2**) in MeCN.

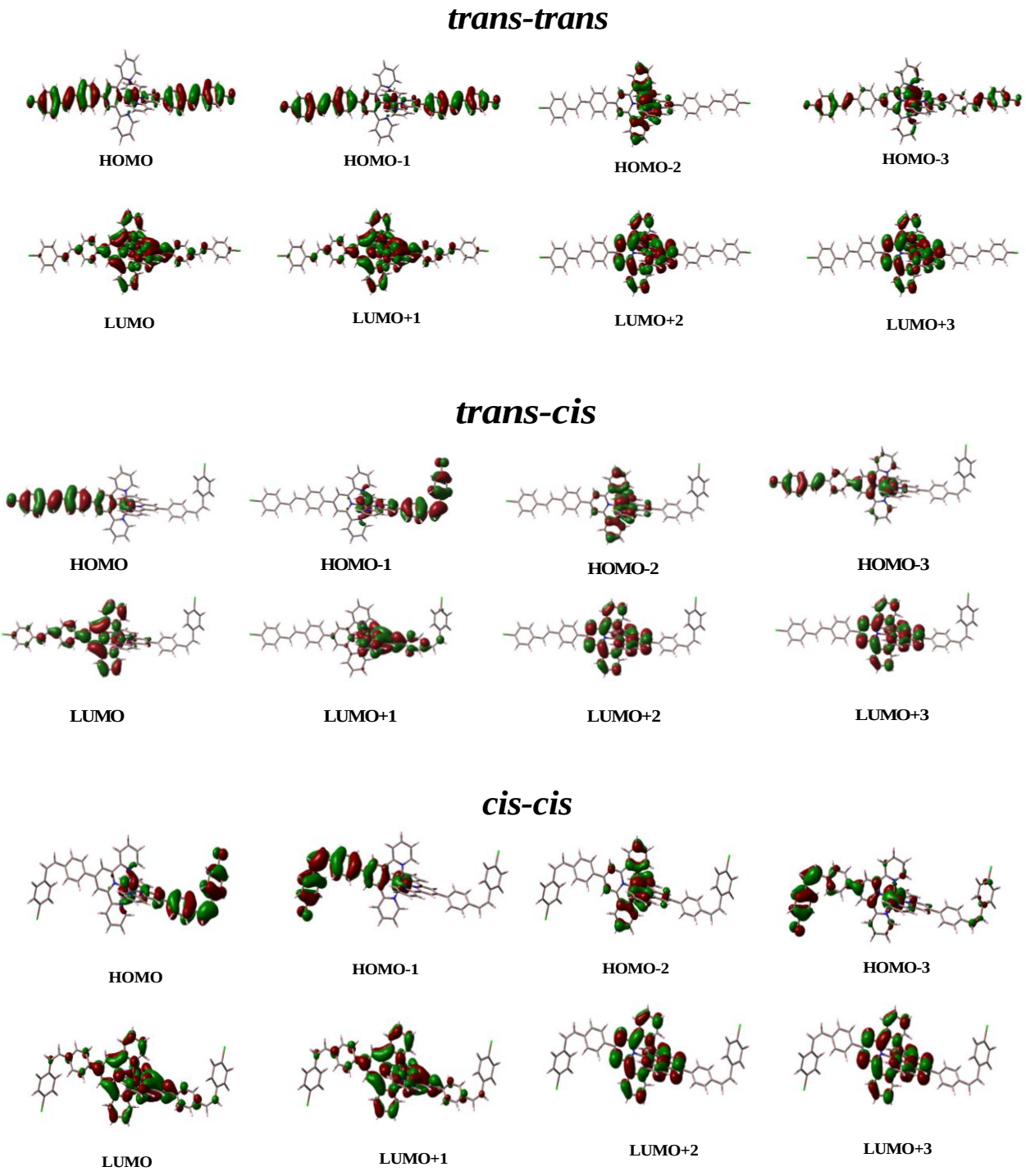

Figure S17. Schematic drawings of the selective frontier molecular orbitals of *trans-trans*, *trans-cis* and *cis-cis* form of $[(Ru(tpy\text{-}pvp\text{-}Cl)_2]^{2+}$ (**3**) in MeCN.

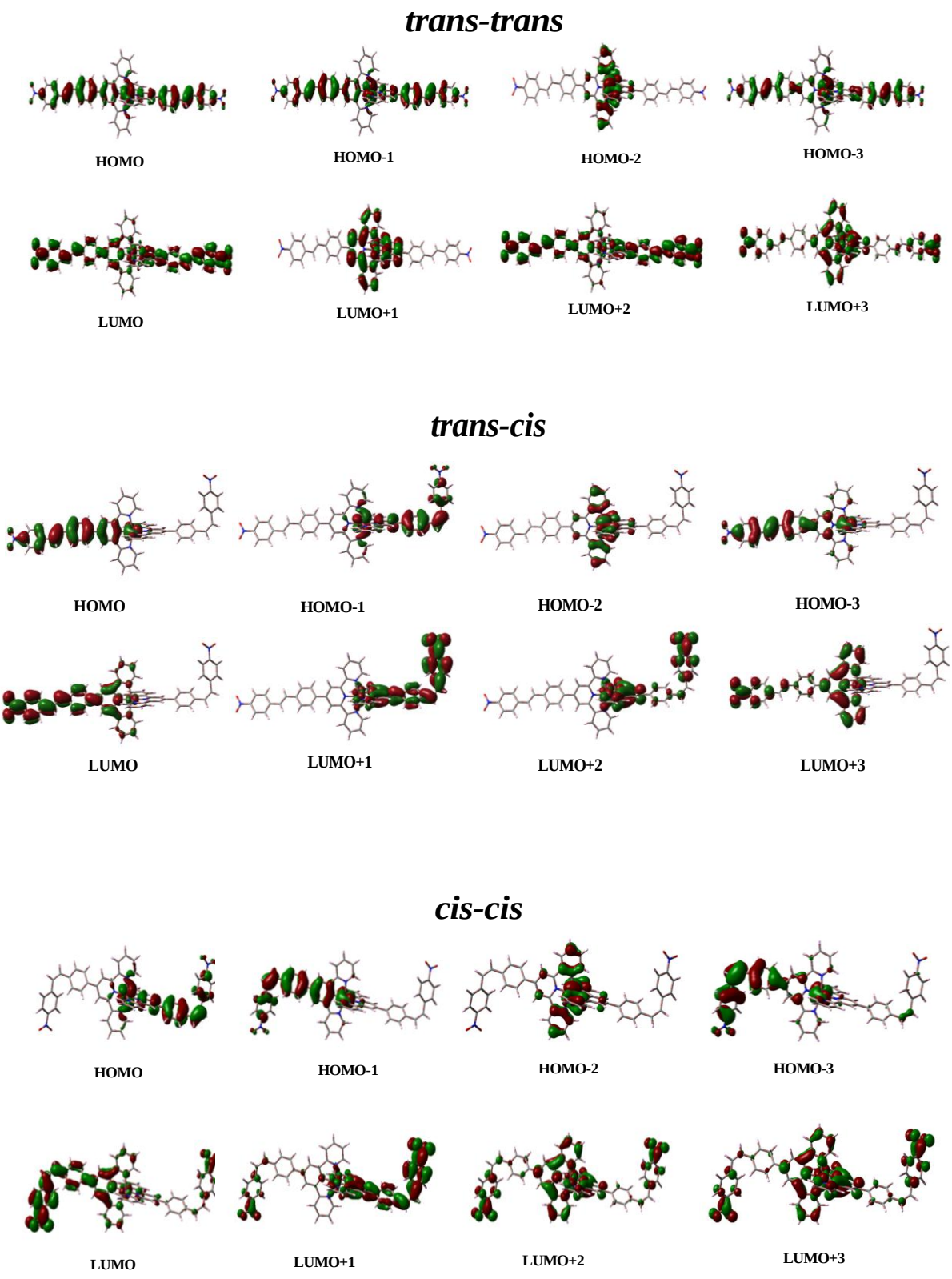

Figure S18. Schematic drawings of the selective frontier molecular orbitals of *trans-trans*, *trans-cis* and *cis-cis* form of $[(Ru(tpy\text{-}pvp\text{-}NO_2)_2]^{2+}$ (**4**) in MeCN.

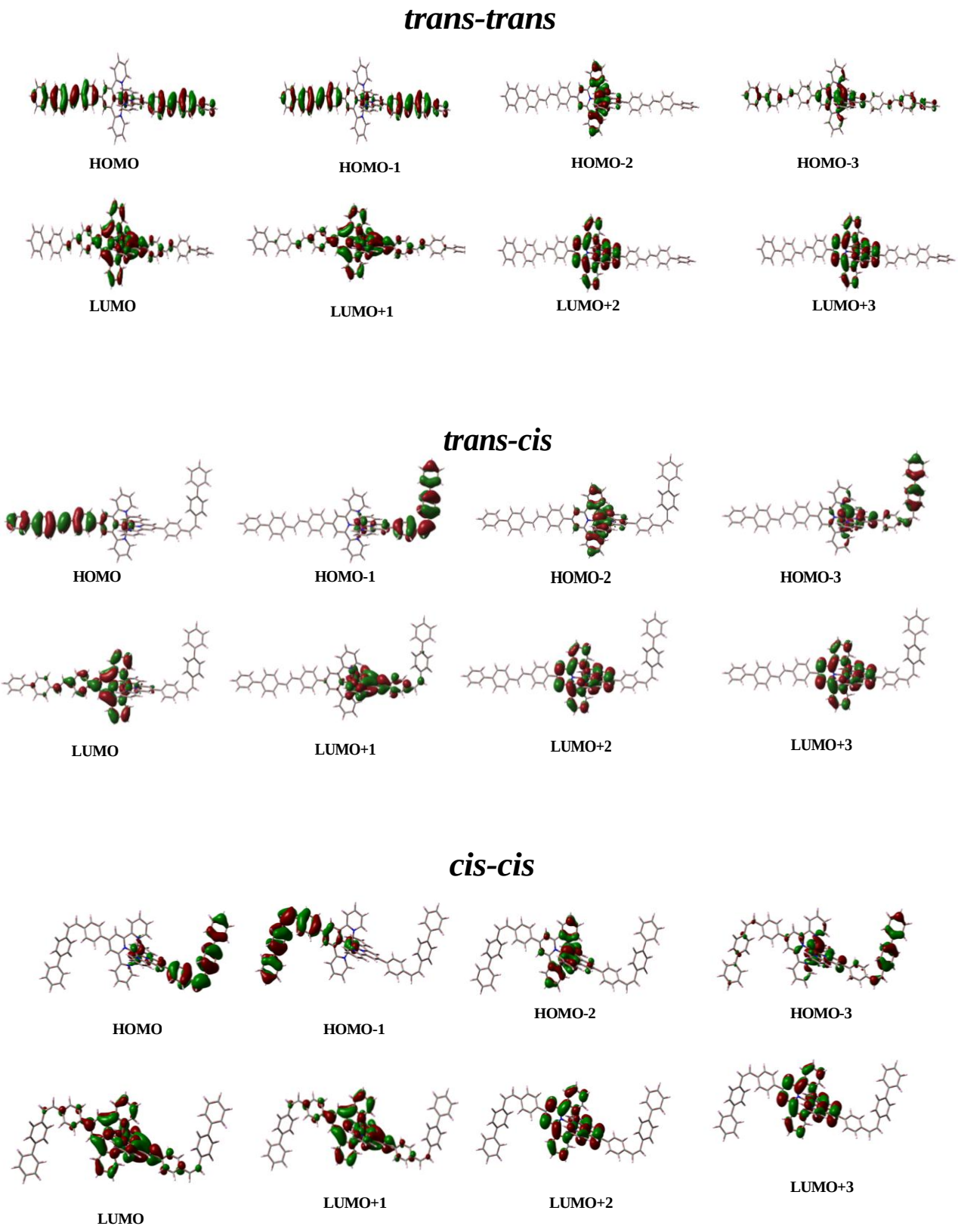

Figure S19. Schematic drawings of the selective frontier molecular orbitals of *trans-trans*, *trans-cis* and *cis-cis* form of $[(Ru(tpy\text{-}pvp\text{-}Ph)_2]^{2+}$ (**5**) in MeCN.

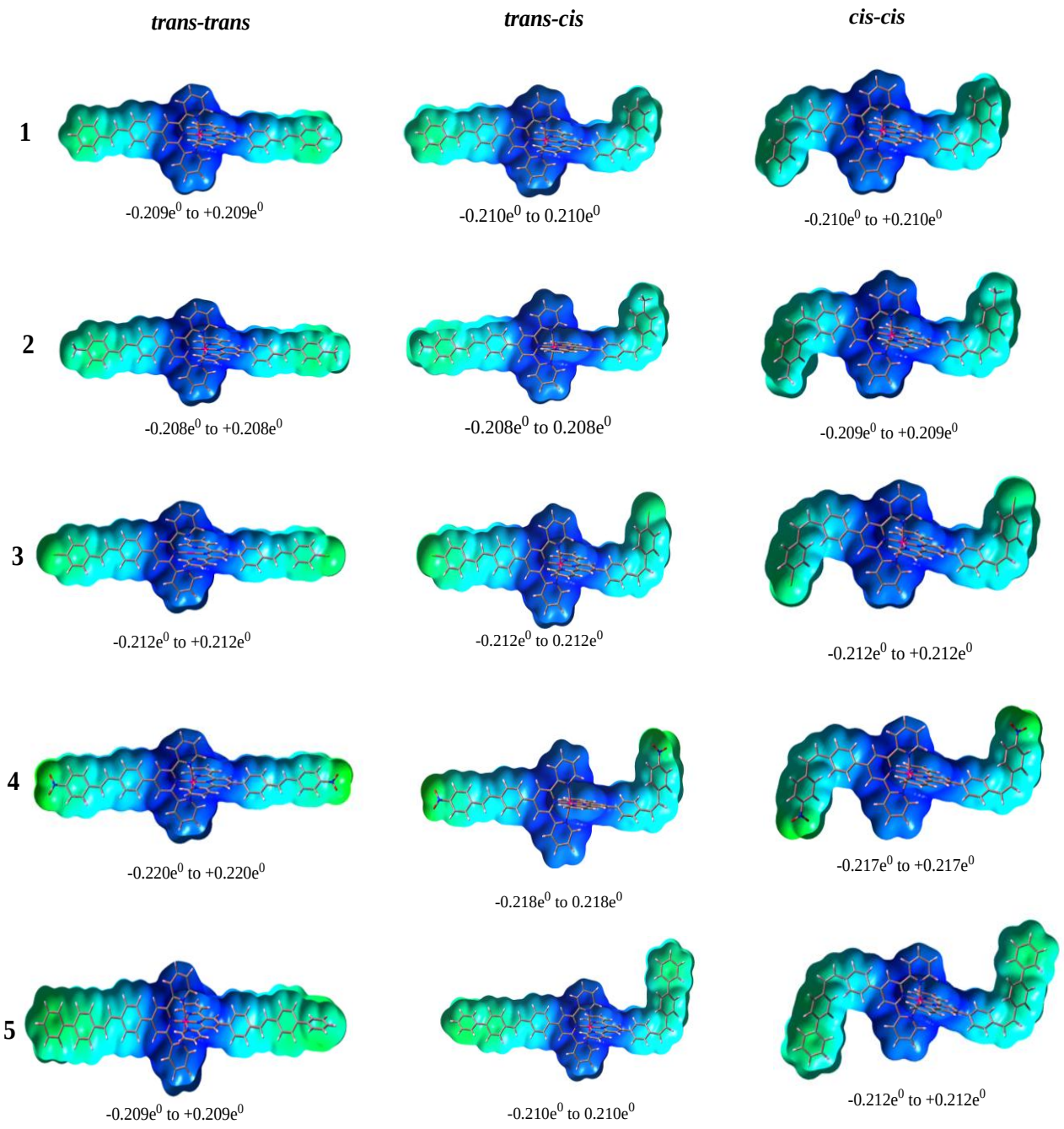

Figure S20. Electrostatic surface potential (ESP) plots of *trans-trans*, *trans-cis* and *cis-cis* forms of **1-5** in MeCN.

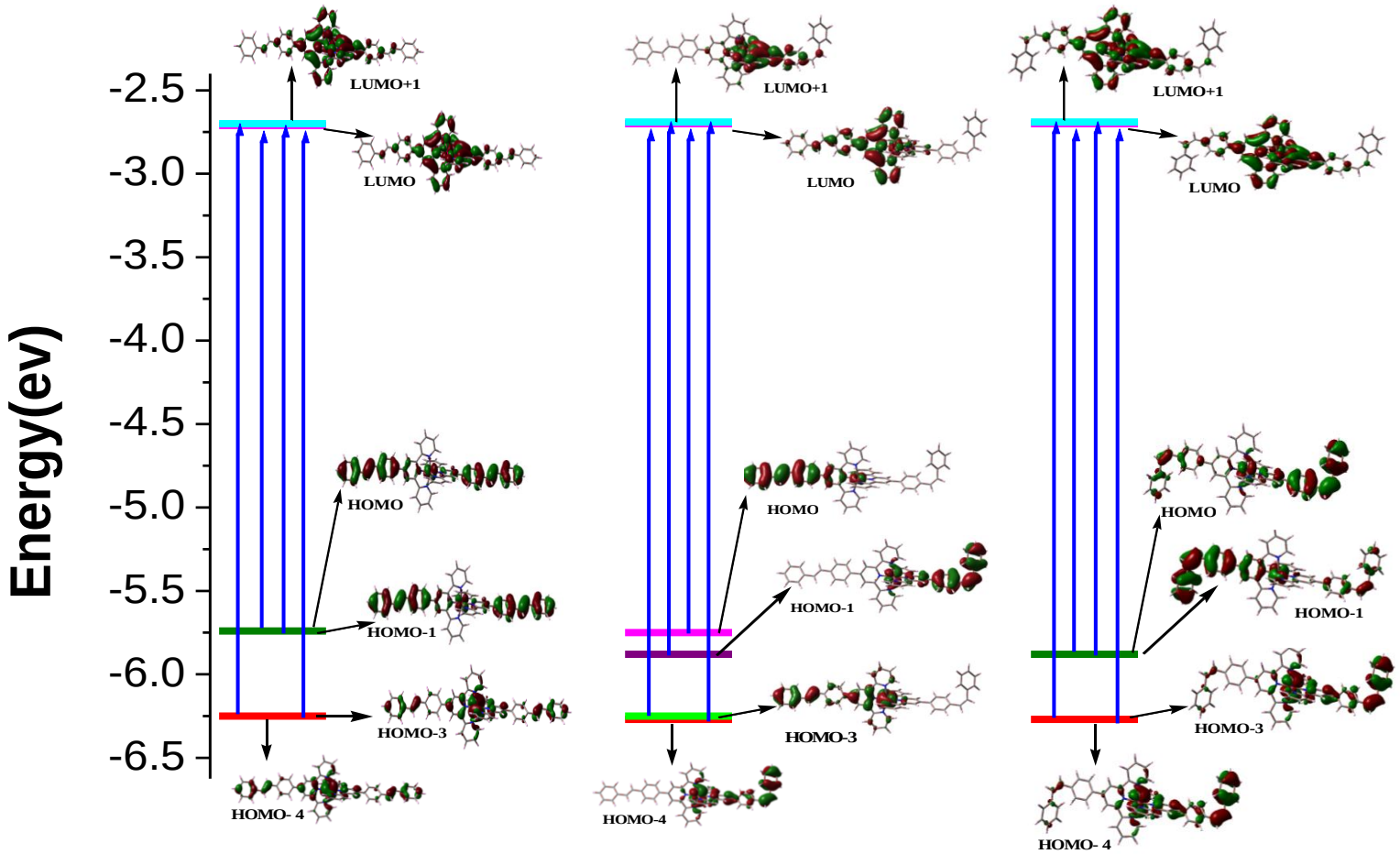

Figure S21. Energy level diagram showing the major transitions that comprise the lowest-energy absorption band for both *trans-trans* (left panel), *trans-cis* (middle panel) and *cis-cis* (right panel) forms of $[(Ru(tpy\text{-}pvp\text{-}H)_2]^{2+}$ (**1**) in MeCN.

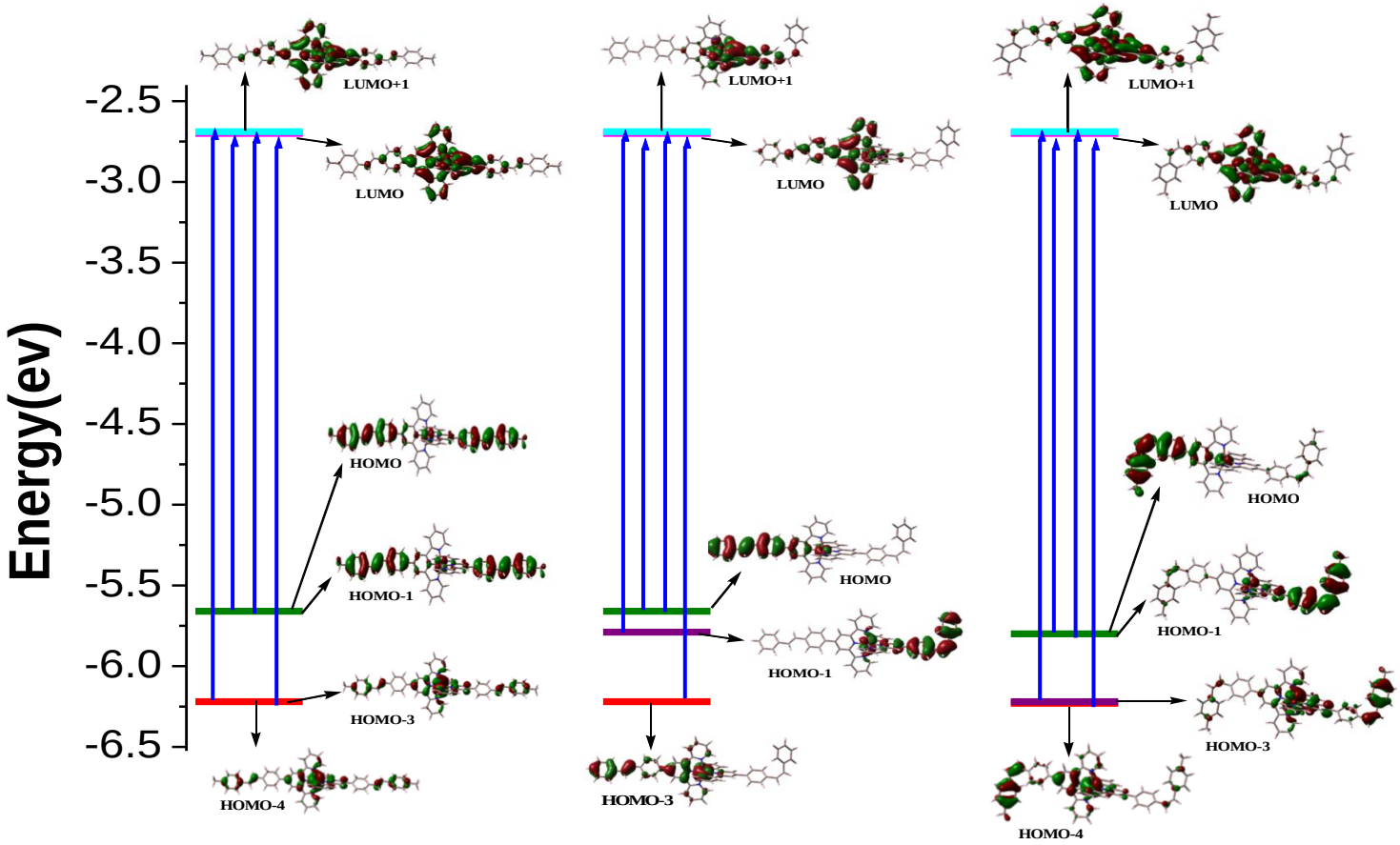

Figure S22. Energy level diagram showing the major transitions that comprise the lowest-energy absorption band for both *trans-trans* (left panel), *trans-cis* (middle panel) and *cis-cis* (right panel) forms of $[(Ru(tpy\text{-}pvp\text{-}Me)_2]^{2+}$ (**2**) in MeCN.

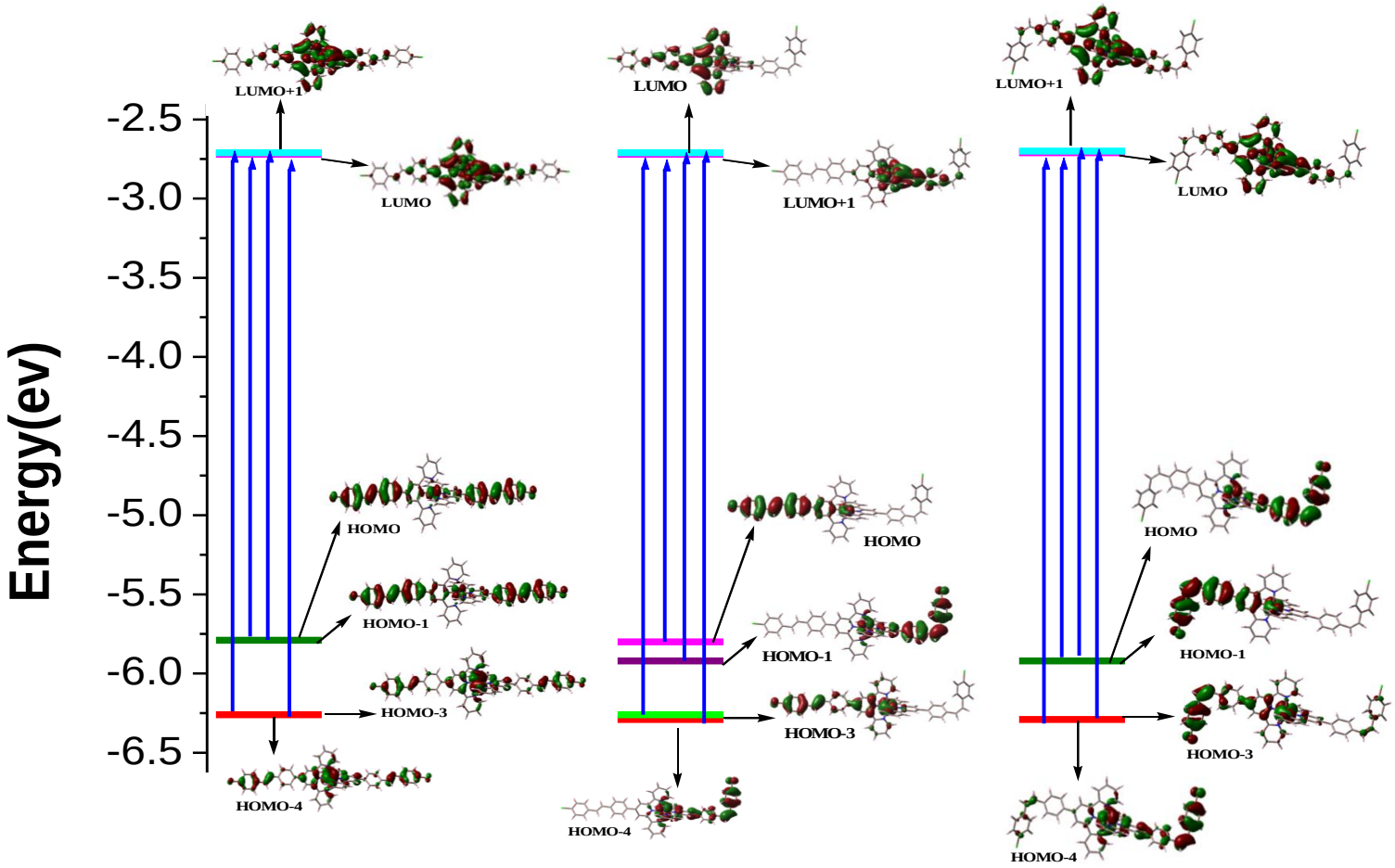

Figure S23. Energy level diagram showing the major transitions that comprise the lowest-energy absorption band for both *trans-trans* (left panel), *trans-cis* (middle panel) and *cis-cis* (right panel) forms of $[(Ru(tpy\text{-}pvp\text{-}Cl)_2]^{2+}$ (**3**) in MeCN.

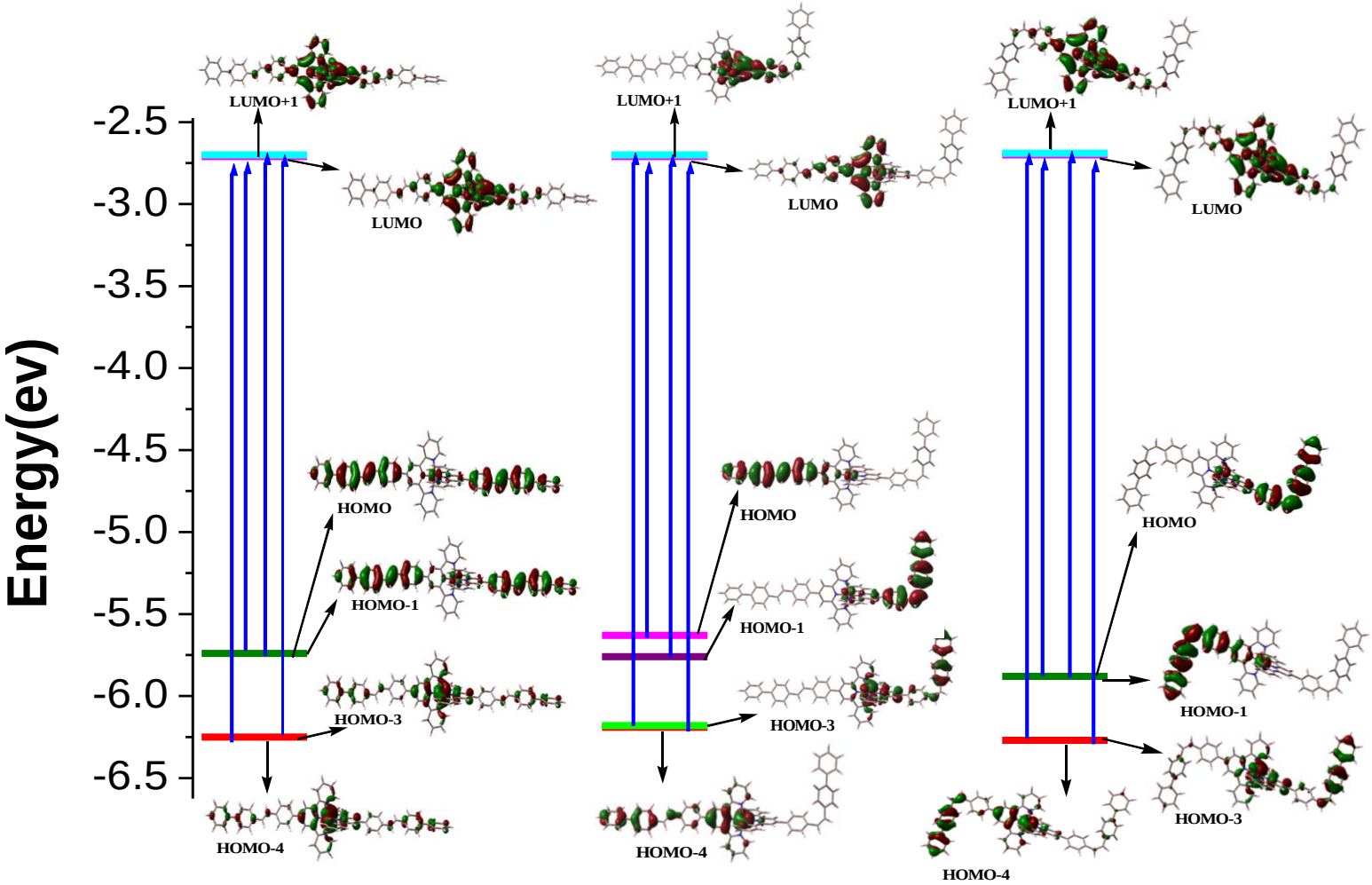

Figure S24. Energy level diagram showing the major transitions that comprise the lowest-energy absorption band for both *trans-trans* (left panel), *trans-cis* (middle panel) and *cis-cis* (right panel) forms of $[(Ru(tpy\text{-}pvp\text{-}Ph)_2]^{2+}$ (**5**) in MeCN.

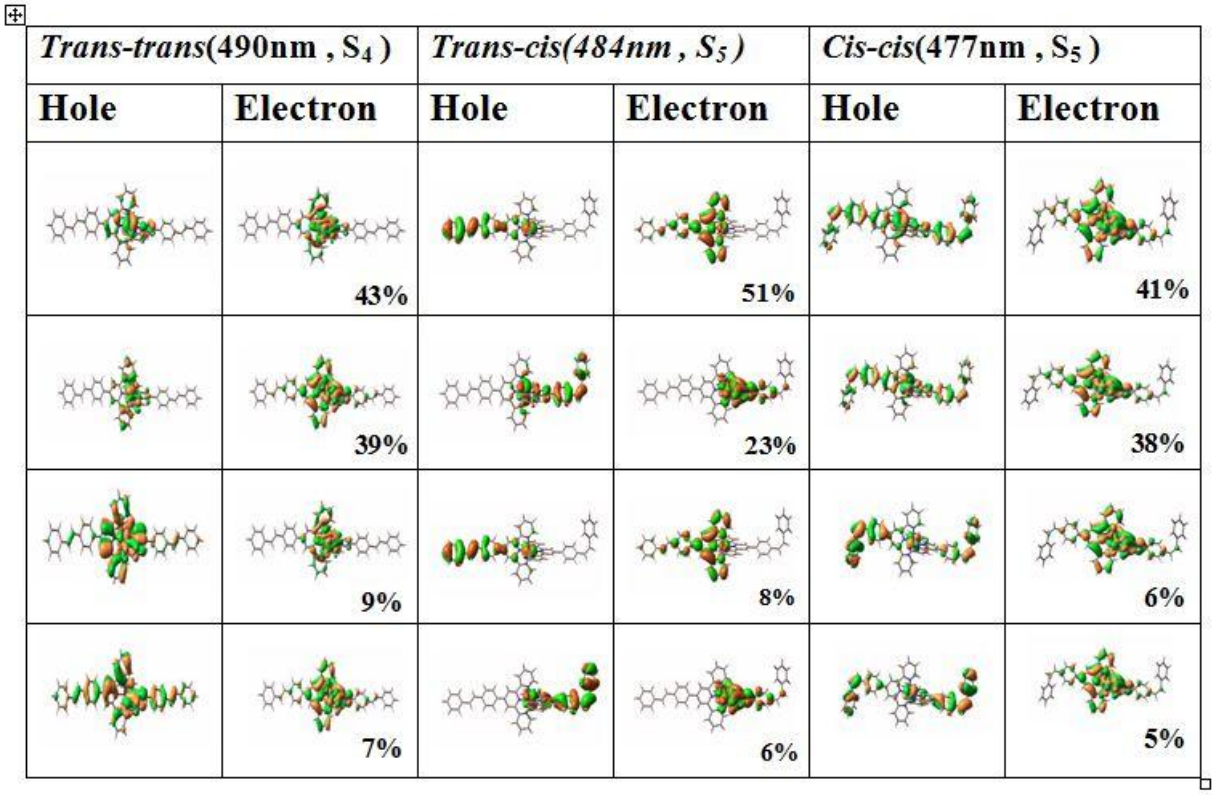

Figure S25. NTOs illustrating the nature of optically active singlet excited states in the absorption bands at 490 nm (S_4) for **1**-*trans-trans*, 484 nm (S_5) for **1**-*trans-cis* and 477 nm (S_5) for **1**-*cis-cis*. The occupied (holes) and unoccupied (electrons) NTO pairs that contribute more than 5% to each excited state are only represented. All transitions are mixed ^{1}MLCT/^{1}IL.

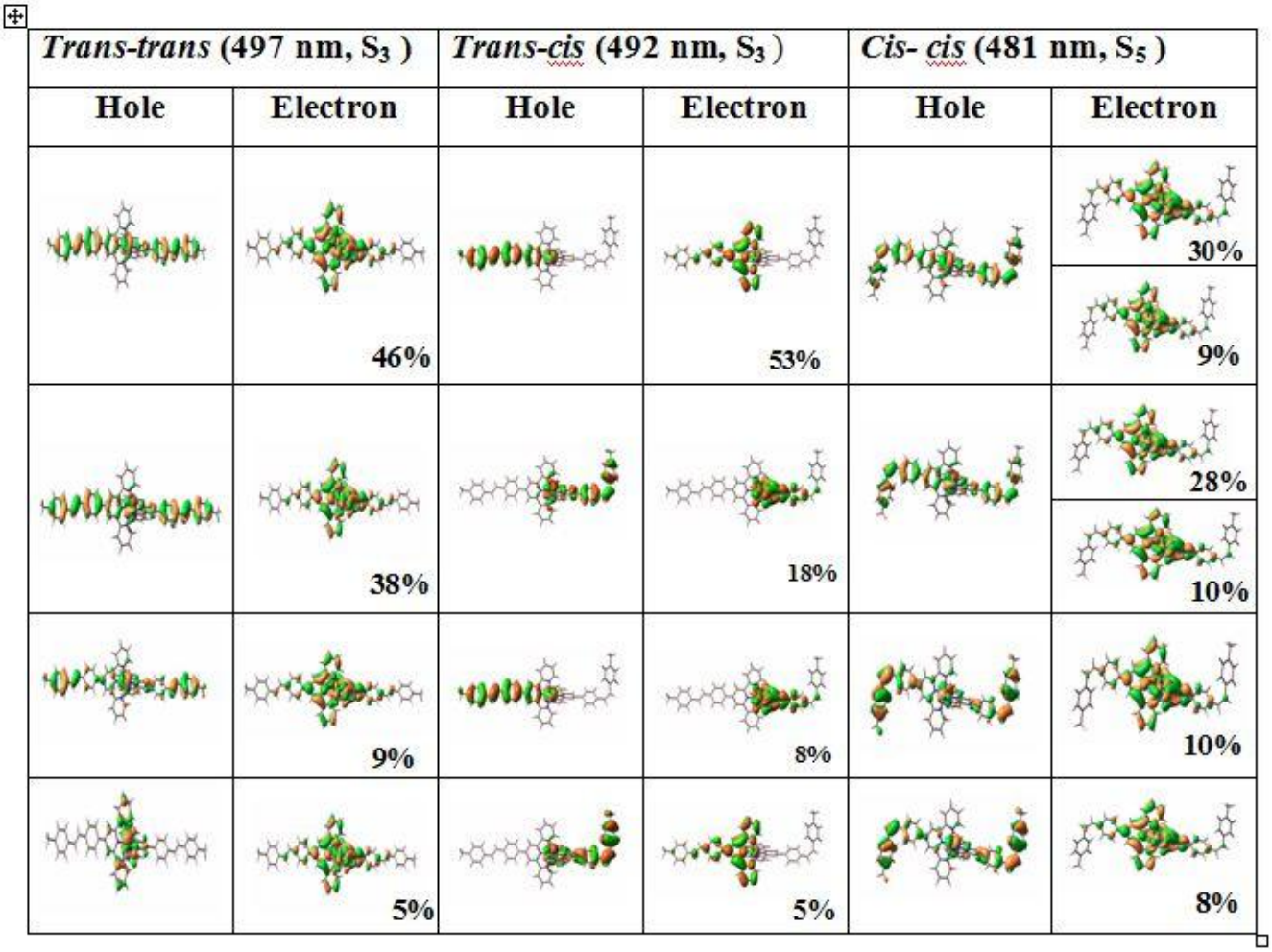

Figure S26. NTOs illustrating the nature of optically active singlet excited states in the absorption bands at 497 nm (S_3) for **2**-*trans*-*trans*, at 492 nm (S_3) for **2**-*trans*-*cis* and 481 nm (S_5) for **2**-*cis*-*cis*. The occupied (holes) and unoccupied (electrons) NTO pairs that contribute more than 5% to each excited state are only represented. All transitions are mixed ^{1}MLCT/^{1}IL.

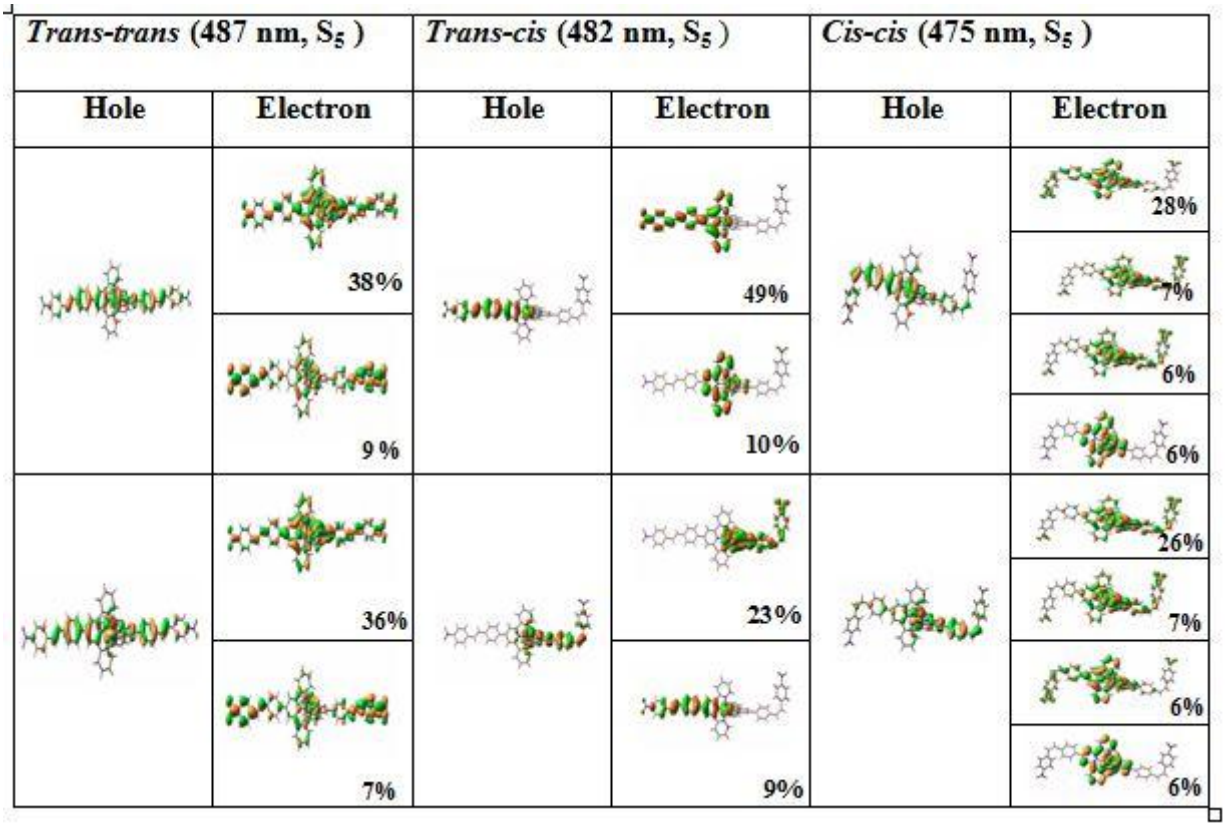

Figure S27. NTOs illustrating the nature of optically active singlet excited states in the absorption bands at 487 nm (S_5) for **4**-*trans*-*trans*, at 482 nm (S_5) for **4**-*trans*-*cis* and 475 nm (S_5) for **4**-*cis*-*cis*. The occupied (holes) and unoccupied (electrons) NTO pairs that contribute more than 5% to each excited state are only represented. All transitions are mixed ^{1}MLCT/^{1}IL.

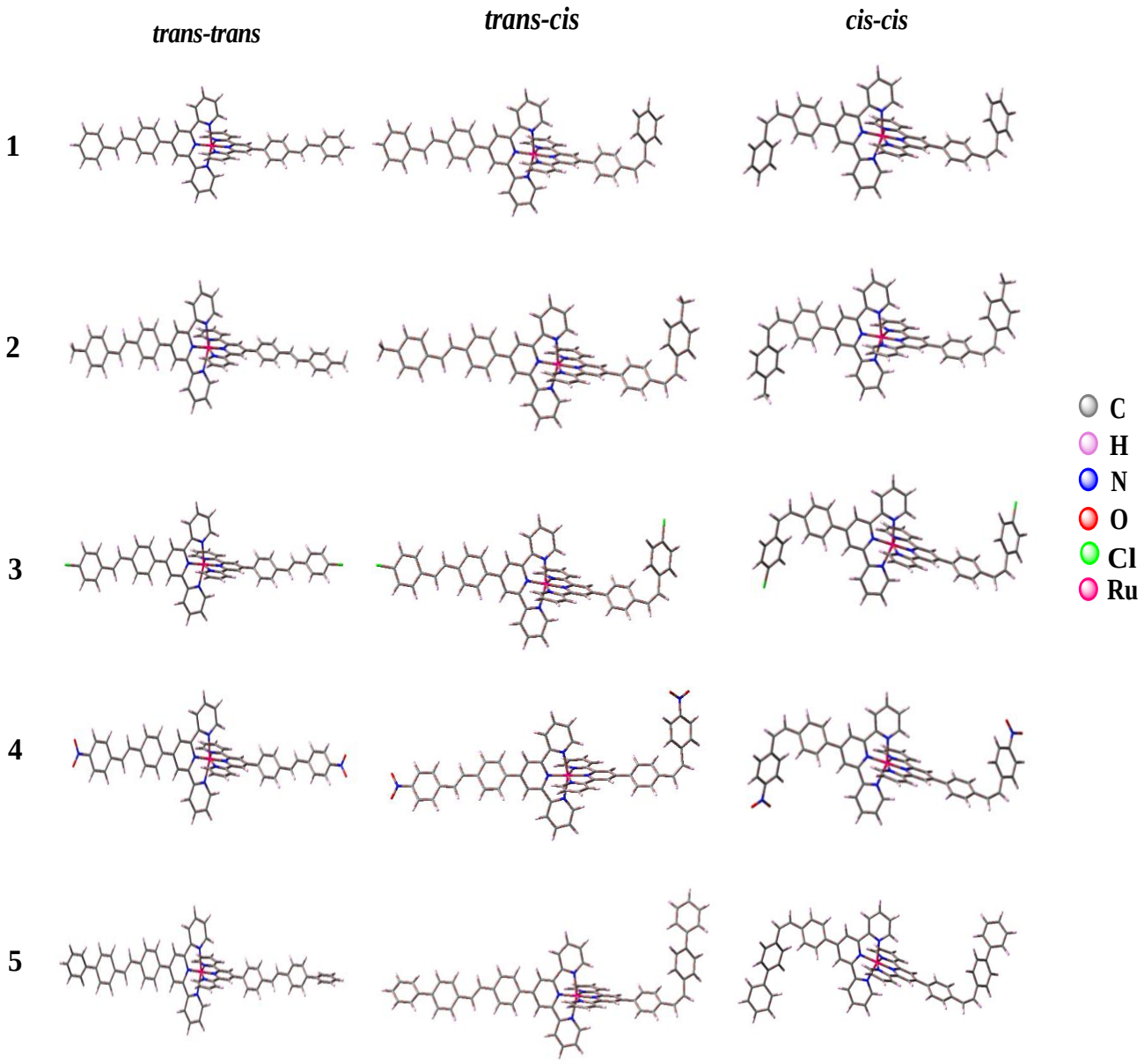

Figure S28. UKS optimized geometries of the *trans-trans*, *trans-cis* and *cis-cis* forms of **1-5** in MeCN.

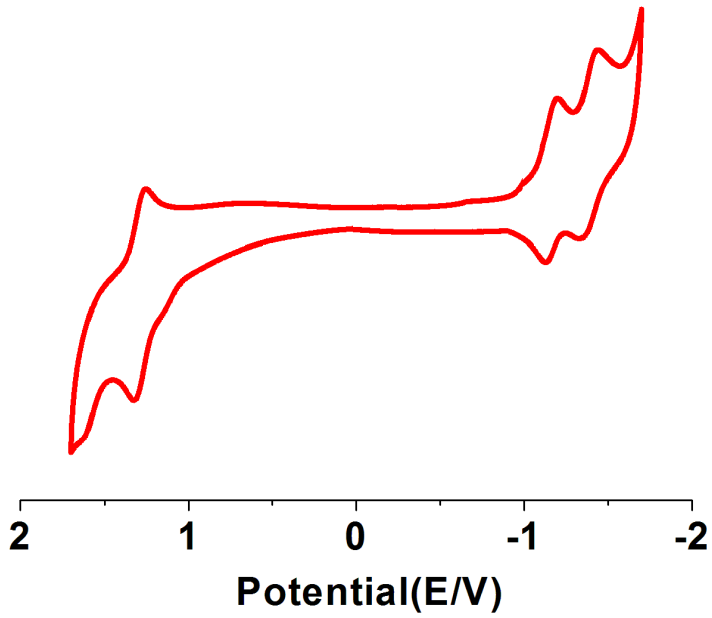

Figure S29. Cyclic voltammogram of **1** in MeCN at a scan rate of 100 mV/s using glassy carbon as the working electrode and Ag/AgCl as the reference electrode.

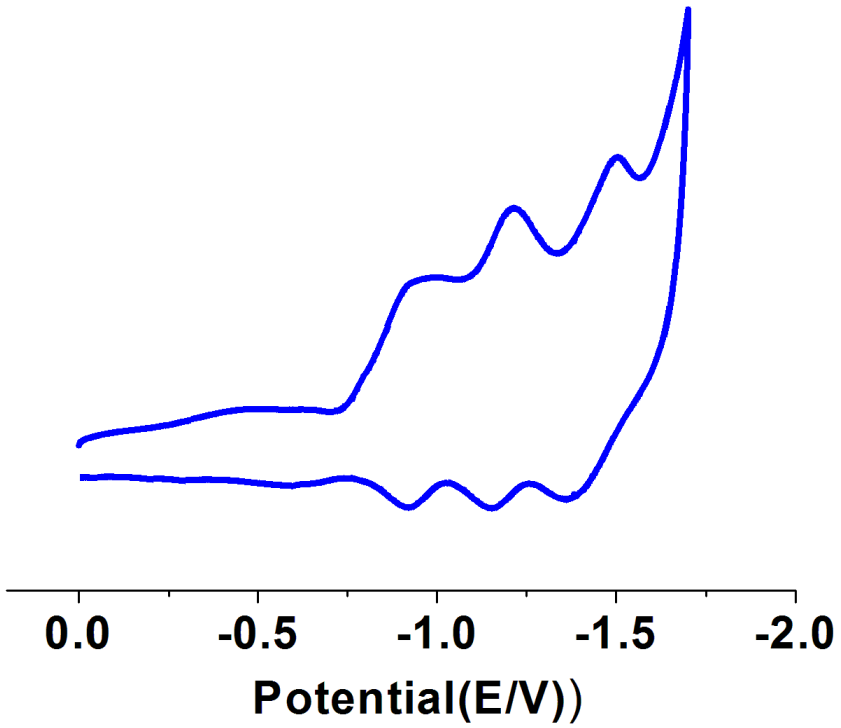

Figure S30. Cyclic voltammogram of **4** in MeCN showing multiple reduction waves in the negative potential at a scan rate of 100 mV/s using glassy carbon as the working electrode and Ag/AgCl as the reference electrode.

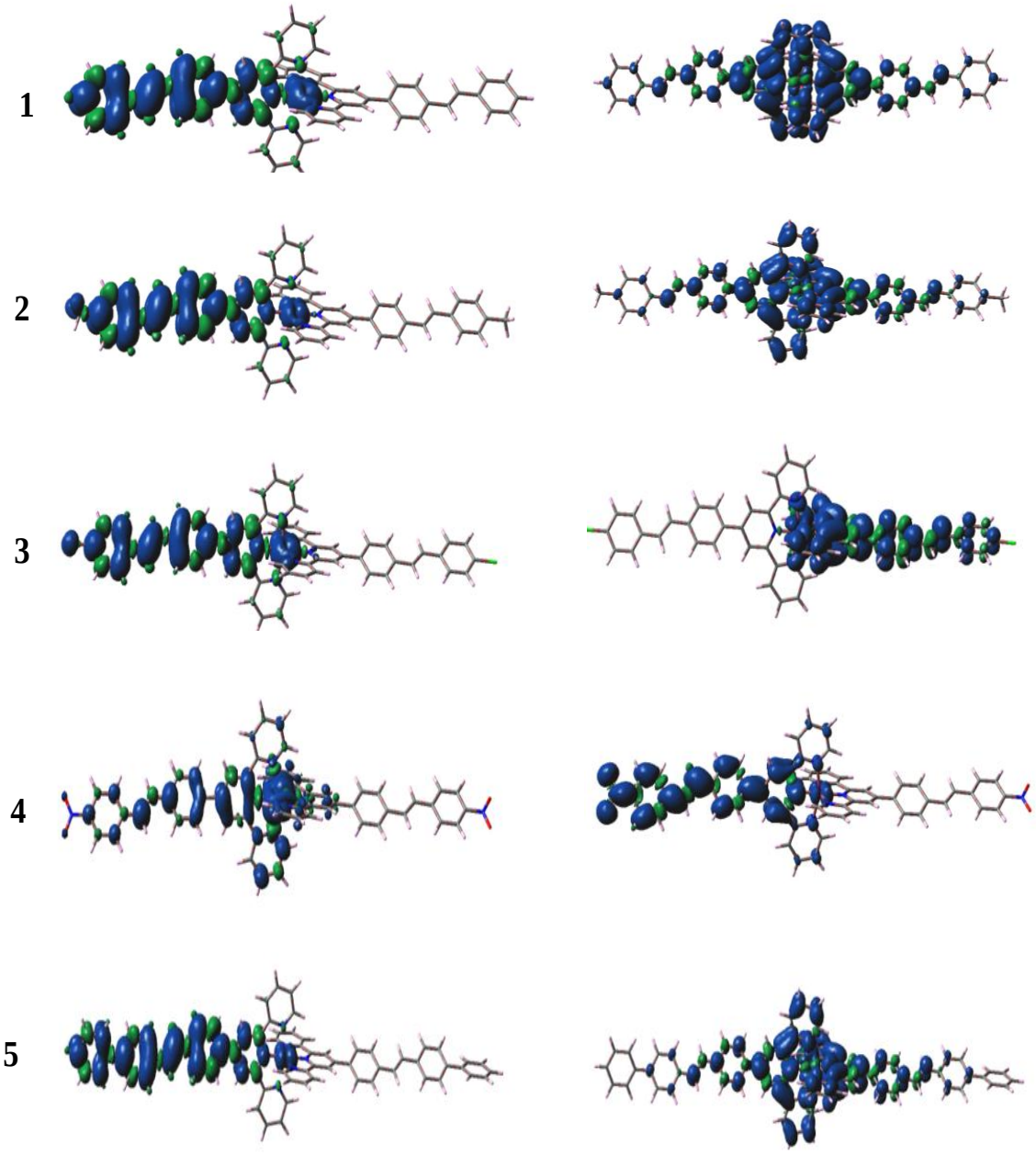

Figure S31. Spin density plots for one-electron oxidized (left panel) and one-electron reduced (right panel) forms of the complexes (**1-5**) in MeCN.

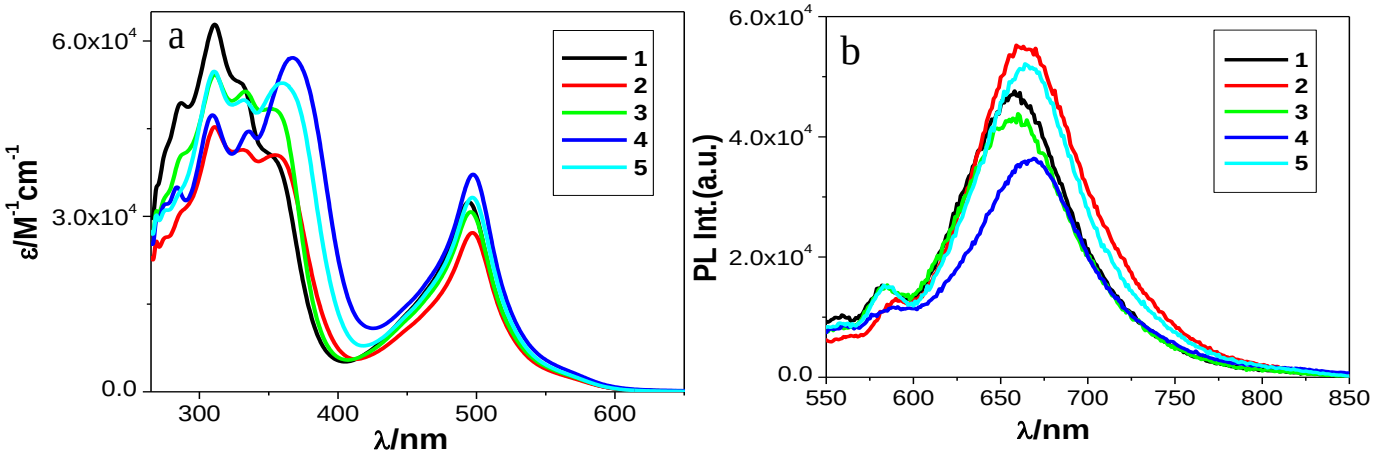

Figure S32. UV-vis absorption (a) and emission (b) spectra of the complexes (**1-5**) in MeCN.

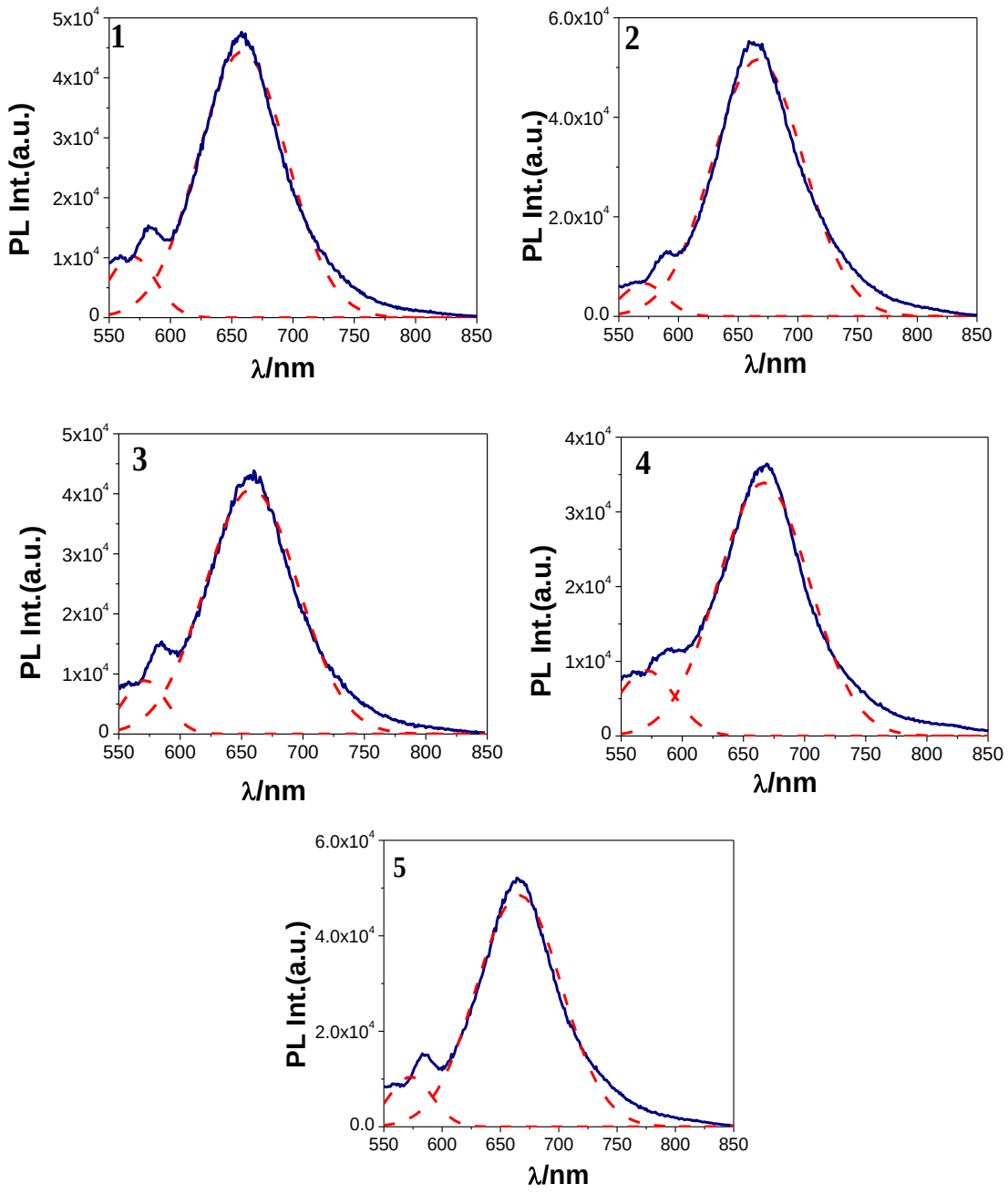

Figure S33. Experimental luminescence spectra (blue) along with their deconvoluted forms (dotted red line) of **1-5** in MeCN.

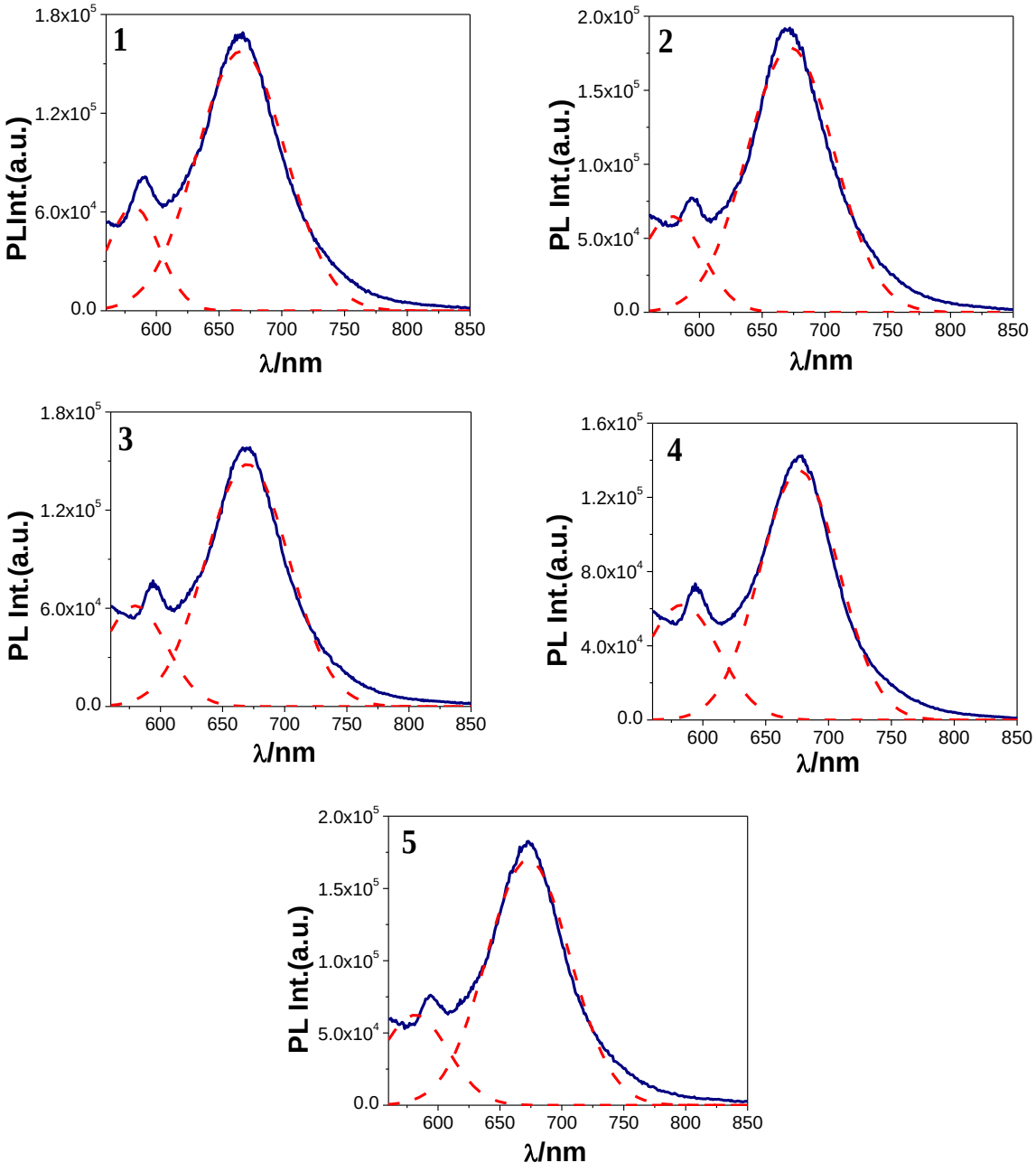

Figure S34. Experimental luminescence spectra (blue) along with their deconvoluted forms (dotted red line) of **1-5** in DMSO.

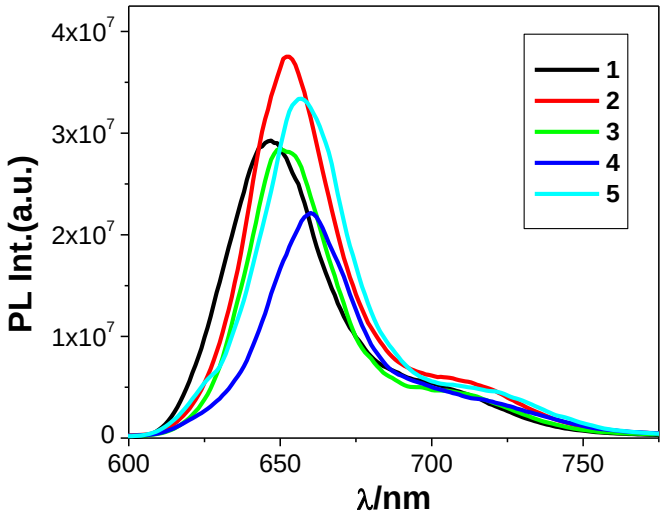

Figure S35. Emission spectra of **1-5** in EtOH-MeOH (4:1, v/v) glass at 77 K.

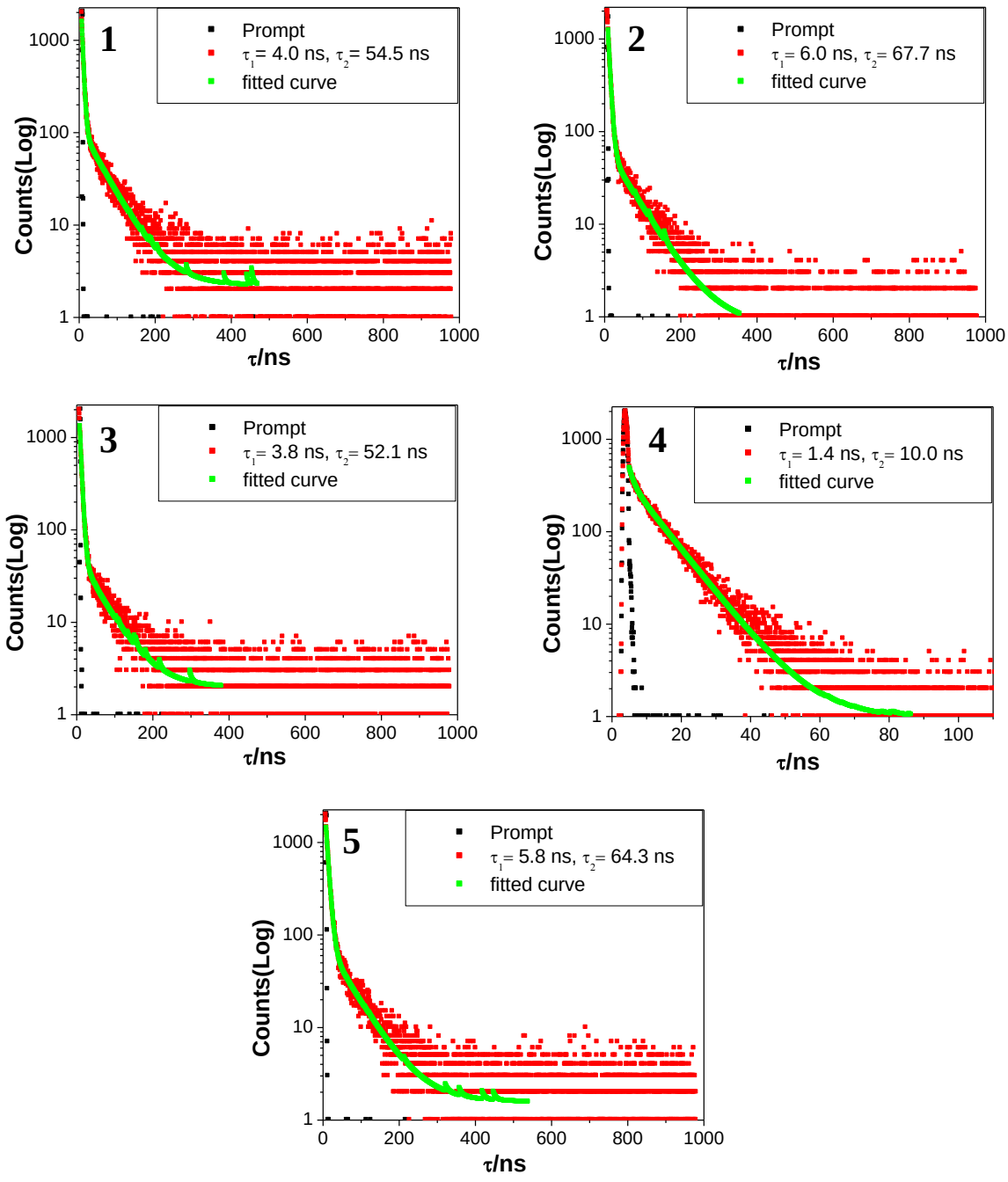

Figure S36. Luminescence decays (λ_{ex} = 450 nm) of **1-5** in MeCN at RT. The insets show the values of the lifetimes of the complexes.

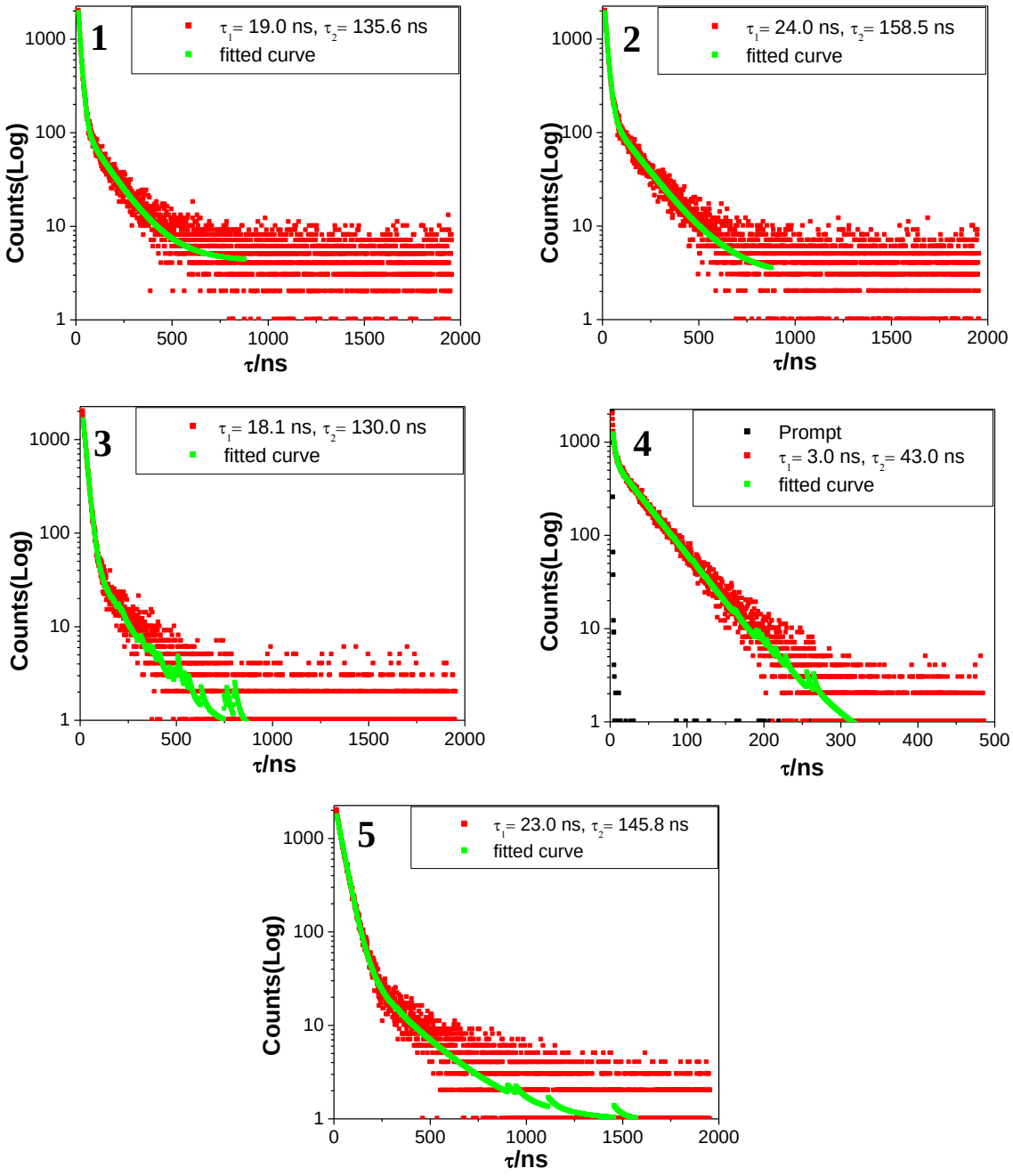

Figure S37. Luminescence decays (λ_{ex} = 450 nm) of **1-5** in DMSO at RT. The insets show the values of the lifetimes of the complexes.

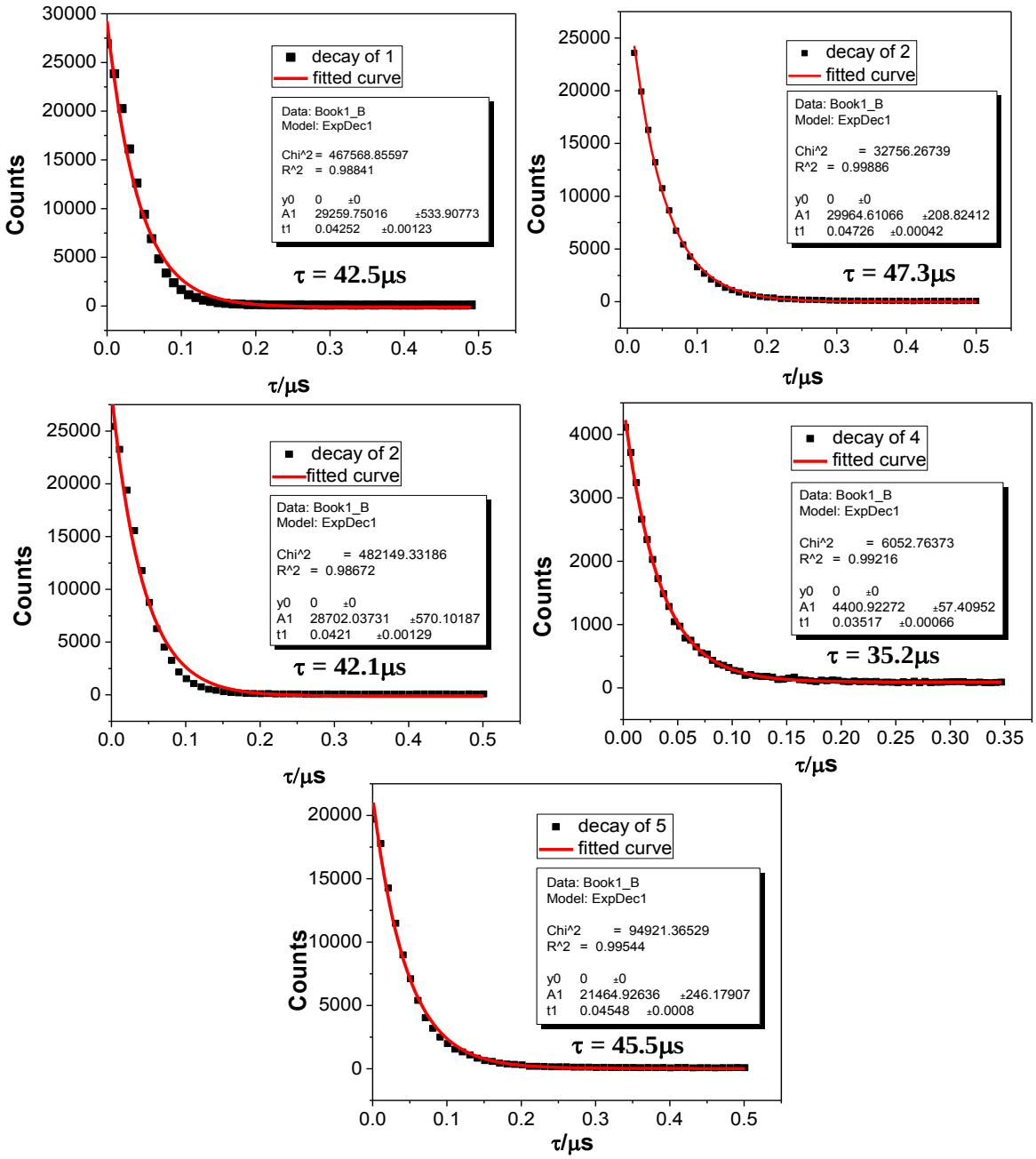

Figure S38. Luminescence decay profiles of the complexes (**1-5**) in 4:1 (v/v) EtOH-MeOH glass at 77 K. Excitation wavelength was 500 nm.

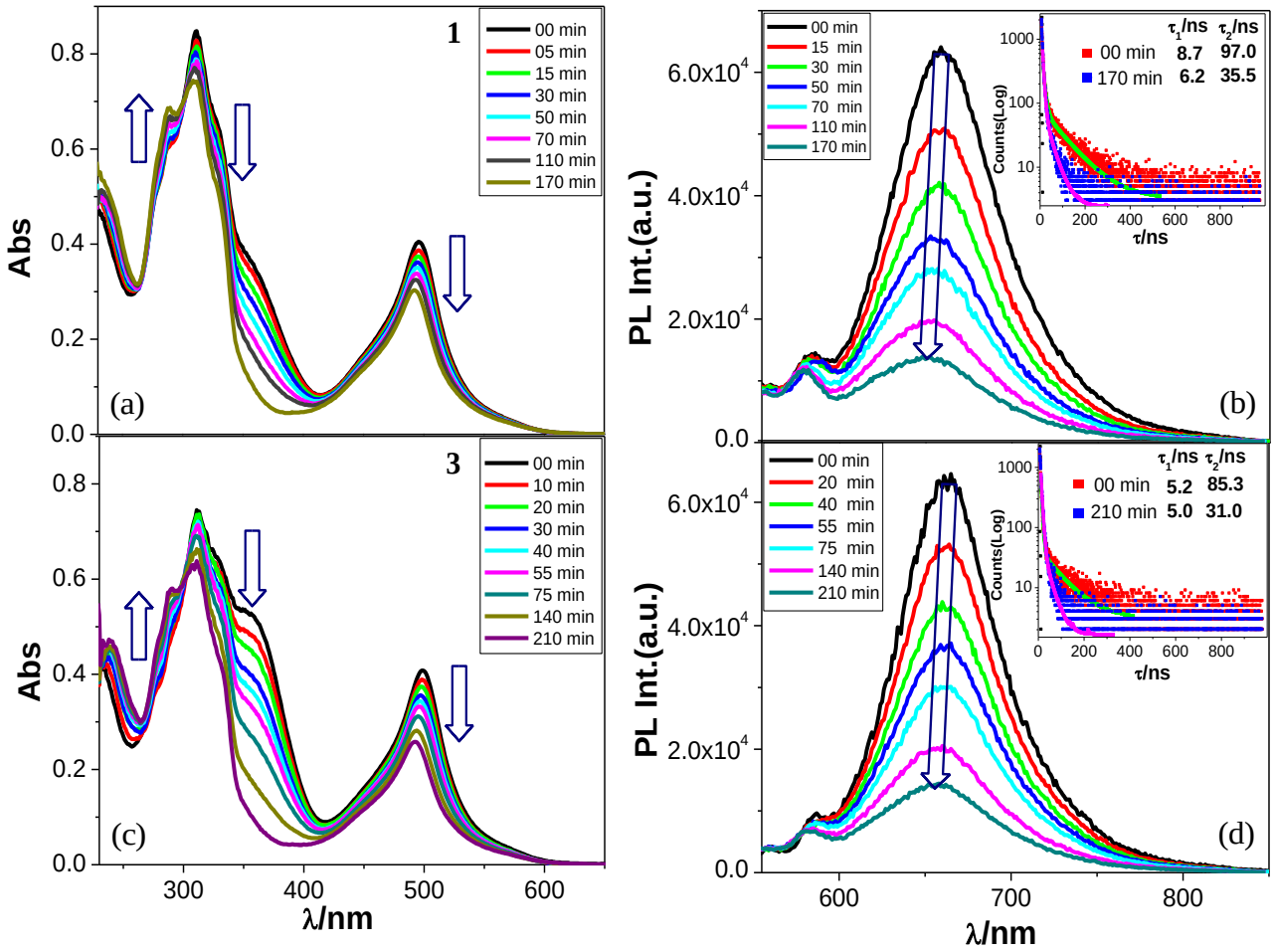

Figure S39. UV-vis absorption and emission spectral changes of **1** (a and b, respectively) and **3** (c and d, respectively) in MeCN-DCM (1:50 v/v) upon irradiation with UV light. Excitation wavelength for recording the emission is 500 nm. Changes in lifetime upon photolysis are shown in the insets.

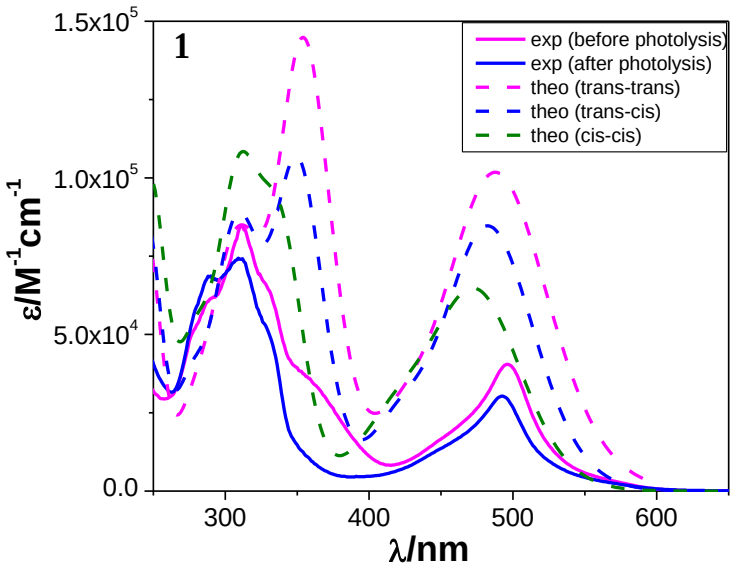

Figure S40. Calculated {dashed lines: *trans-trans* (pink), *trans-cis* (blue), *cis-cis* (green)} and observed (solid lines) absorption spectra of **1**in MeCN.

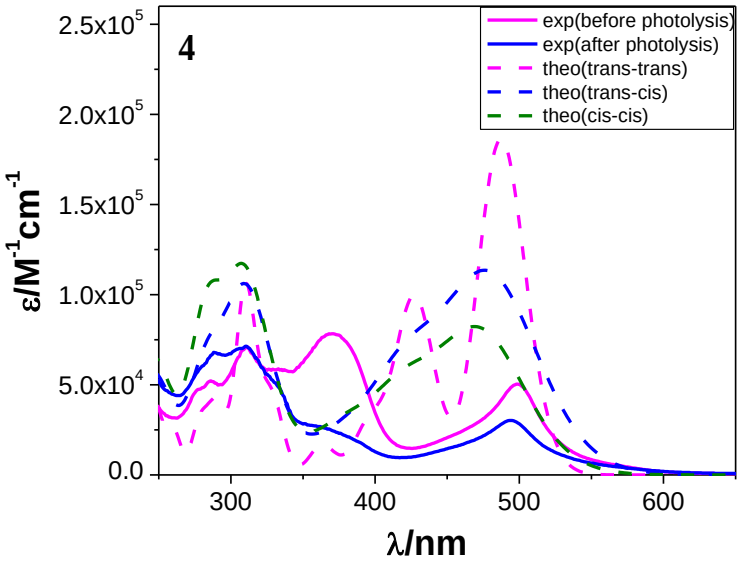

Figure S41. Calculated {dashed lines: *trans-trans* (pink), *trans-cis* (blue), *cis-cis* (green)} and observed (solid lines) absorption spectra of **4** in MeCN.

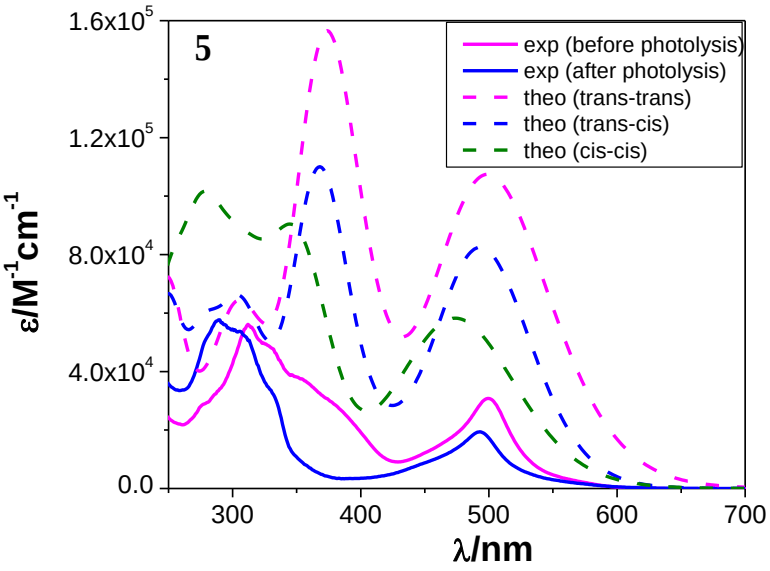

Figure S42. Calculated {dashed lines: *trans-trans* (pink), *trans-cis* (blue), *cis-cis* (green)} and observed (solid lines) absorption spectra of **5** in MeCN.

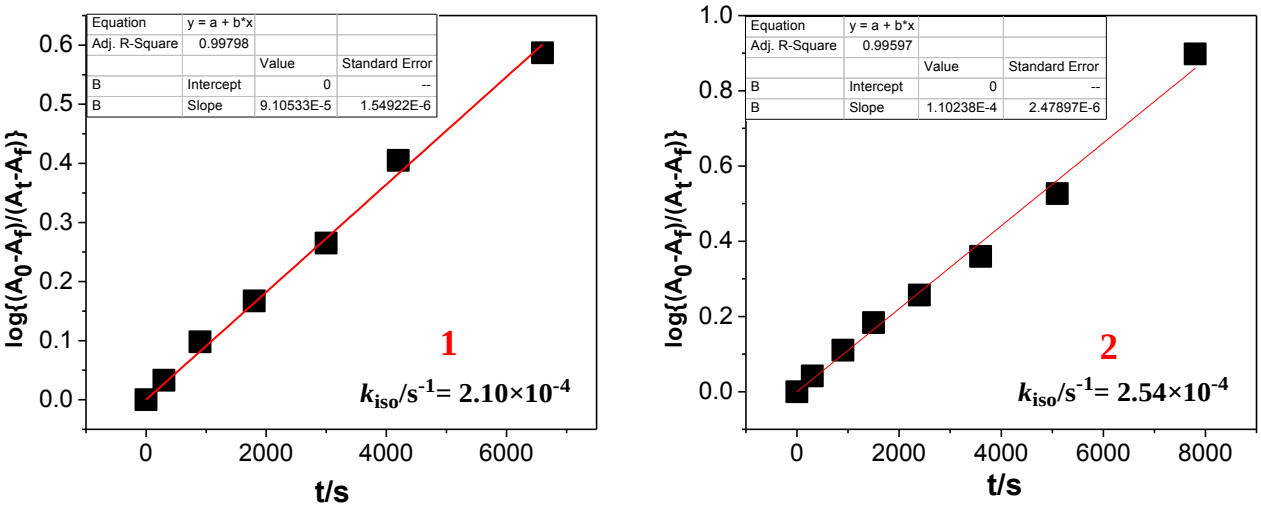

Figure S43. Linear plot of $\log(A_0-A_f)/(A_t-A_f)$ *vs*. time for $[Ru(tpy\text{-}pvp\text{-}H)_2]^{2+}$ (**1**) and $[(Ru(tpy\text{-}pvp\text{-}Me)_2]^{2+}$ (**2**) gives the value of rate constant of photo-isomerization process.

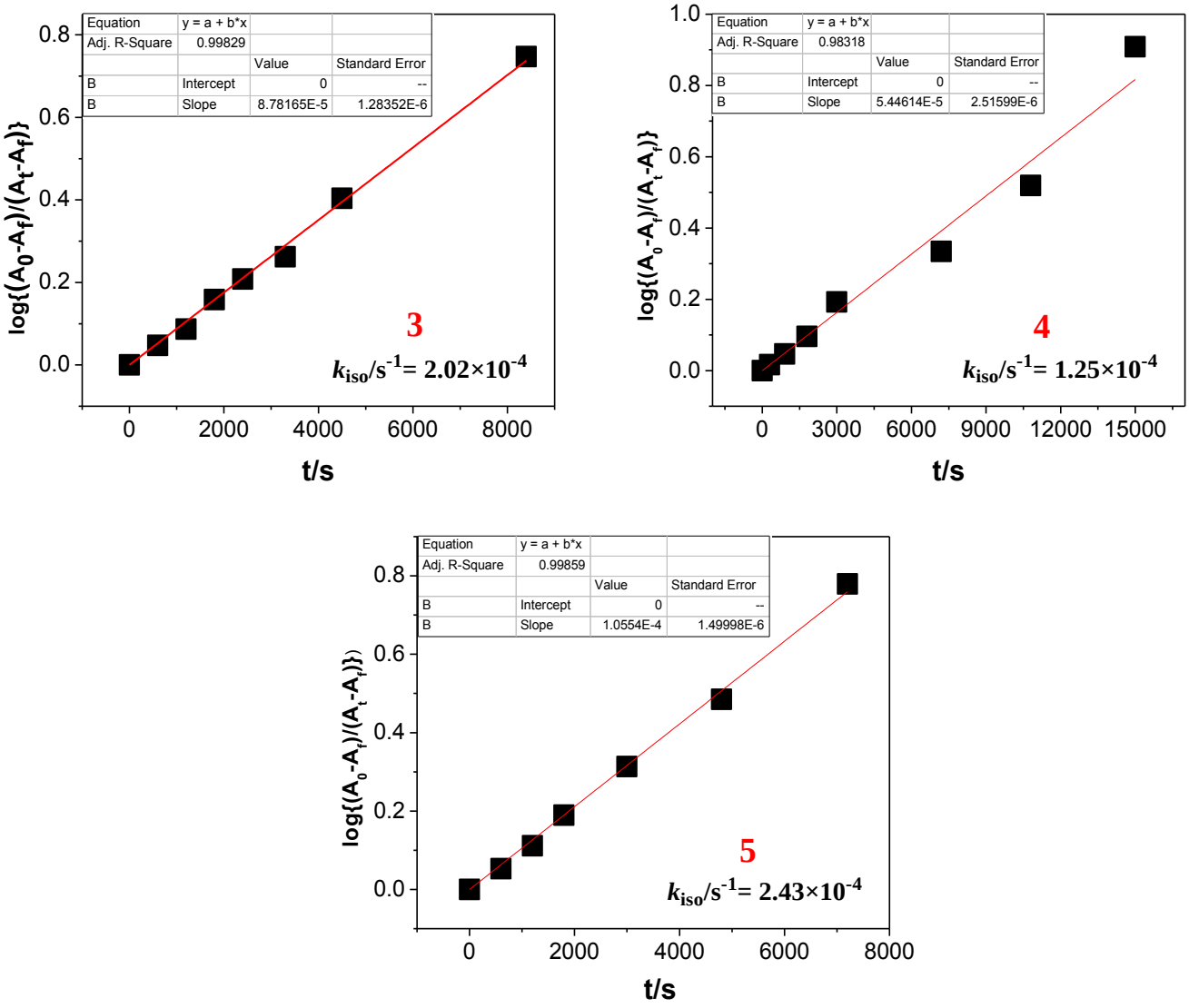

Figure S44. Linear plot of $\log(A_0-A_f)/(A_t-A_f)$ *vs.* time for $[Ru(tpy\text{-}pvp\text{-}Cl)_2]^{2+}$ (**3**), $[(Ru(tpy\text{-}pvp\text{-}NO_2)_2]^{2+}$ (**4**) and $[(Ru(tpy\text{-}pvp\text{-}Ph)_2]^{2+}$ (**5**) gives the value of rate constant of photo-isomerization process.

REFERENCES

S1. Gille, K.; Knoll, H.; Quitzsch, K. Rate constants of the thermal cis-trans isomerization of azobenzene dyes in solvents, acetone/water mixtures, and in microheterogeneous surfactant solutions. *Int. J. Chem. Kinet.* **1999**, *31*, 337-350.

S2. Otsuki, J.; Suwa, K.; Narutaki, K.; Sinha, C.; Yoshikawa, I.; Araki, K. Photochromism of 2-(phenylazo)imidazoles. *J. Phys. Chem A* **2005**, *109*, 8064-8069.

S3. Frisch, M. J.; Trucks, G. W.; Schlegel, H. B.; Scuseria, G. E.; Robb, M. A.; Cheeseman, J. R.; Scalmani, G.; Barone, V.; Mennucci, B.; Petersson, G. A.; Nakatsuji, H.; Caricato, M.; Li, X.; Hratchian, H. P.; Izmaylov, A. F.; Bloino, J.; Zheng, G.; Sonnenberg, J. L.; Hada, M.; Ehara, M.; Toyota, K.; Fukuda, R.; Hasegawa, J.; Ishida, M.; Nakajima, T.; Honda, Y.; Kitao, O.; Nakai, H.; Vreven, T.; Jr. Montgomery, J. A., Peralta, J. E.; Ogliaro, F.; Bearpark, M.; Heyd, J. J.; Brothers, E.; Kudin, K. N.; Staroverov, V. N.; Kobayashi, R.; Normand, J.; Raghavachari, Rendell, K. A.; Burant, J. C.; Iyengar, S. S.; Tomasi, J.; Cossi, M.; Rega, N.; Millam, J. M.; Klene, M.; Knox, J. E.; Cross, J. B.; Bakken, V.; Adamo, C.; Jaramillo, J.; Gomperts, R.; Stratmann, R. E.; Yazyev, O.; Austin, A. J.; Cammi, R.; Pomelli, C.; Ochterski, J. W.; Martin, R. L.; Morokuma, K.; Zakrzewski, V. G.; Voth, G. A.; Salvador, P.; Dannenberg, J. J.; Dapprich, S.; Daniels, A. D.; Farkas, Ö.; Foresman, J. B.; Ortiz, J. V.; Cioslowski, J.; Fox, D. J. Gaussian 09, revision A.02; Gaussian Inc.: Wallingford, CT, 2009.

S4. Becke, A. D. Density functional thermochemistry. III. The role of exact exchange. *J. Chem. Phys.* **1993**, *98*, 5648-5652.

S5. Lee, C. T.; Yang, W. T.; Parr, R. G. Development of the Colle-Salvetti correlation-energy formula into a functional of the electron density. *Phys. Rev. B* **1988**, *37*, 785-789.

S6. (a) Andrae, D.; Haeussermann, U.; Dolg, M.; Stoll, H.; Preuss, H. Energy-adjusted *ab initio* pseudopotentials for the second and third row transition elements. *Theor. Chim. Acta.* **1990**, *77*, 123-141. (b) Fuentealba, P.; Preuss, H.; Stoll, H.; Szentpaly, L. V. A proper account of core-polarization with pseudopotentials: single valence-electron alkali compounds. *Chem. Phys. Lett*. **1989**, *89*, 418-422.

S7. Hay, P. J.; Wadt, W. R. *Ab initio* effective core potentials for molecular calculations. Potentials for K to Au including the outermost core orbitals. *J. Chem. Phys.* **1985**, *82*, 299-310.

S8. Casida, M. E.; Jamorski, C.; Casida, K. C.; Salahub, D. R. Molecular excitation energy to high- lying bound state from time-dependent density functional response theory:

charecterization and correction of the time dependent local density approximation ionization thresold. *J. Chem. Phys.* **1998**, *108*, 4439-4449.

S9. Stratmann, R. E.; Scuseria, G. E.; Frisch, M. J. An efficient implementation of time-dependent density-functional theory for the calculation of excitation energies of large molecules. *J. Chem. Phys.* **1998**, *109*, 8218-8224.

S10. Walters, V. A.; Hadad, C. M.; Thiel, Y.; Colson, S. D.; Wiberg, K. B.; Johnson, P. M.; Foresman, J. B. Assignment of the A State in Bicyclobutane. The Multiphoton ionization spectrum and calculations of transition energies *J. Am. Chem. Soc.* **1991**, *113*, 4782-4791.

S11. (a) Tomasi, J.; Mennucci, B.; Cammi, R. Quantum Mechanical Continuum Solvation Models. *Chem. Rev*. **2005**, *105*, 2999-3094. (b) Cossi, M.; Scalmani, G.; Rega, N.; Barone, V. New developments in the polarizable continuum model for quantum mechanical and classical calculations on molecules in solution. *J. Chem. Phys*. **2002**, *117*, 43-54.

S12. Caricato, M.; Mennucci, B.; Tomasi, J.; Ingrosso, F.; Cammi, R.; Corni, S.; Scalmani, G. Formation and relaxation of excited states in solution: a new time dependent polarizable continuum model based on time dependent density functional theory. *J. Chem. Phys*. **2006**, *124*, 124520-124530.

S13. Mennucci, B.; Cappelli, C.; Guido, C. A.; Cammi, R.; Tomasi, J. Structures and properties of electronically excited chromophores in solution from the polarizable continuum model coupled to the time-dependent density functional theory. *J. Phys. Chem. A* **2009**, *113*, 3009.

S14. Dennington, R. II.; Keith T.; Millam, J. *Gauss View 3*; Semichem, Inc.: Shawnee Mission, KS, 2007.

S15. O Boyle, N. M.; Tenderholt, A. L.; Langner, K. M. cclib: A library for package-independent computational chemistry algorithms. *J. Comput. Chem*. **2008**, *29*, 839.

S16. SAINT (version 6.02), SADABS (version 2.03); Bruker AXS Inc.: Madison, WI, 2002.

S17. Sheldrick, G. M. SHELXL-97, *Program for the Refinement of crystal Structures*; University of Göttingen: Göttingen, Germany, 1997.

S18. SHELXTL, (version 6.10); Bruker AXS Inc.: Madison, WI, 2002.

S19. Spek, A. L. Single-crystal structure validation with the program PLATON. *J. Appl. Cryst.* **2003**, *36*, 7-13.